

Cluster Populations in Abell 2125 and 2218

Karl Rakos

Institute for Astronomy, University of Vienna, A-1180, Wien, Austria; karl.rakos@chello.at

James Schombert

Department of Physics, University of Oregon, Eugene, OR 97403; js@abyss.uoregon.edu

ABSTRACT

We combine new narrow band photometry with archival WFPC2 data for A2218 ($z=0.18$) and A2125 ($z=0.25$), two clusters with intermediate redshifts but very different cluster properties, in order to examine the evolution of galaxy populations. A2218 is a dense, elliptical-rich cluster (Bautz-Morgan type II) similar to Coma in its evolutionary appearance; whereas, A2125 is a less dense, more open cluster (Bautz-Morgan type II-III), although similar in richness to A2218. The color-magnitude relation indicates that A2125 has a more developed blue population than A2218 (the Butcher-Oemler effect), although both clusters have significant numbers of blue galaxies (ranging in star formation rates from normal, star-forming disks to starburst systems) as compared to a present-day cluster. The colors of the red populations are identical in A2125 and A2218 and well fit by passive evolution models. We are able, for the first time, to combine archived WFPC2 images with our narrow band photometry for a color, morphological and structural analysis of the blue Butcher-Oemler population. We find the blue population to composed of two sub-populations, a bright, spiral population and a fainter, dwarf starburst population. A2125 is richer in bright starburst systems, apparently induced by the cluster's younger dynamical state. In addition, a majority of the S0 population in A2125 and A2218 is composed of bulge+disk systems, whereas, nearby clusters such as Coma are composed primarily of lenticulars (pure disk S0's). The structural parameters of the S0 bulges in A2125/A2218 are identical to the structure parameters of cluster ellipticals suggesting that the disks of some S0's in intermediate redshift clusters are stripped away with the leftover bulges evolving into present-day ellipticals.

Subject headings: galaxies: evolution — galaxies: stellar content — galaxies: elliptical

1. INTRODUCTION

Photometry of distant cluster populations can be used to explore many problems in the area of galaxy evolution (see recent review by Dressler 2003). Topics including color evolution, the Butcher-Oemler effect, cD galaxy construction and S0 formation have all been investigated through detailed photometry of galaxies in rich clusters. However, in recent years, cluster studies using spectroscopy have gained prominence due to the growth in multi-fiber instruments. This has added line indices measurements and kinematic information to that available as new inputs to our growing community of galaxy modelers (van Dokkum *et al.* 2001), but photometry has the advantage of deeper limiting magnitude and spatial resolution while still maintaining spectrophotometric quality with properly selected filter sets.

For the past decade, our team has applied a set of narrow band filters, centered on the 4000Å break (a modified Strömgren system), to study the behavior of the near-blue continuum in galaxies over a range of environments and redshifts. Our technique varies from other photometric studies in that, not only are the filters narrower and focused on continuum regions of a galaxy’s spectral distribution, but the filters are also ‘redshifted’ to each cluster’s velocity to avoid k-corrections and provide for photometric membership selection. The interpretation of narrow band colors differs from spectral line work in that they can determine the mean star formation rates averaged over the past few Gyrs rather than instantaneous rates as given by emission lines. Thus, we find that continuum studies can compliment the work of spectral studies, particularly with respect to the star formation history of galaxies.

The Strömgren system used herein consists of four filters (uz, vz, bz, yz) which are centered around the 4000Å break. The advantages to the Strömgren system for galaxy evolution are: 1) cluster membership is assigned based on photometric criteria, thus the ability to study lower luminosity galaxies in distant clusters which are too faint for spectroscopy, 2) the mean star formation rate is defined by spectrophotometric criteria, and 3) for quiescent objects (i.e. ellipticals and S0’s), our color indices can resolve age and metallicity effects (Rakos & Schombert 2005). Through principal component analysis (Steindling, Brosch & Rakos 2001), we can divide our sample by color into E (old), S- (passive, S0-type), S (disk star formation rates) and S+ (starburst or unusually high star formation rates). These spectrophotometric classifications are used to identify and study the blue population in clusters (the Butcher-Oemler effect), while the remaining red population can be examined for metallicity and age effects.

In our past studies, we have observed the blue and red populations in a handful of intermediate redshift clusters. Our goal has been to study 1) the color-magnitude (mass-metallicity) relation for the red population and mean age of ellipticals as a function of luminosity (mass), 2) identify the blue population and determine its photometric properties, 3) examine the distribution of the red and blue populations in the clusters environment, and 4) compare the changes in cluster populations as a function of cluster type and redshift. In this work, now armed with a larger set of analysis tools, we compare two clusters (A2125 and A2218) which have similar lookback times (about 2 Gyrs), yet contrasting cluster dynamical states. In addition, both clusters have deep HST WFPC2 imaging allowing us to compare colors with morphological and structural information. This unique dataset of combined ground-based narrow band colors and space-based imaging will allow us, for the first time, to compare color and morphological evolution in two different cluster environments. This paper is organized into nine sections; a description of the observations (both ground and space-based), spectrophotometric classification, morphological classification, structural parameters, multi-color diagrams, the color-magnitude relation, color evolution of the red population, the blue fraction and the characteristics of the blue population. Throughout this work we have assumed a Benchmark cosmology ($\Omega_M = 0.3$, $\Omega_\Lambda = 0.7$, $\Omega_k = 0.0$, $H_0 = 75$).

2. OBSERVATIONS

The photometry for this project was obtained on the KPNO 4m over two nights (26/27 Jun 2001). The instrument used was T2KB at prime focus which resulted in a plate scale of 0.48 arcsecs per pixel. The field of view was 14.3 arcmins square which corresponds to 2.4 Mpc for A2218 and 3.1 Mpc for

A2125. Both nights were clear with moderate seeing (0.8 arcsecs). Each cluster was exposed through four dithered frames of 600 secs each for a total of 2,400 secs per filter. Reduction used overscan bias subtraction and dome flat fields. The flatten frames displayed a small gradient across the field of view (on the level of 4%), however the flatfields removed all small features and photometry over small regions of a few tens of arcsecs were not affected by this problem. Calibration was obtained through spectrophotometric standards taken through the night.

Object selection was based on the clear identification of sources in all four filters (uz , vz , bz , yz , see §3.1) at the 3σ level. Atmospheric absorption plus CCD sensitivity meant that detection in the bluest uz filter was the defining factor for inclusion in the final sample. Over 80% of the sample is brighter than $yz = 21$ (5500Å) with the faintest objects having magnitudes of $yz = 22$. A total of 153 galaxies were identified in all four filters for A2125 and 277 galaxies in A2218. The sample is complete to $yz = 21$ mag (corresponding to -18.4 in A2218 and -19.1 in A2125 using the Benchmark Model cosmology). Typical errors at the completeness limit were 0.11 in $uz - yz$ and 0.05 in $vz - yz$ and $bz - yz$. All the raw data is available at the author’s narrow band website (<http://abyss.uoregon.edu/~js>).

In addition to our ground based photometry, both A2125 and A2218 have been imaged by the Hubble Space Telescope WFPC2 system. A2218 has recent special attention by the HST imaging teams since it is a well known gravitational lens cluster (Kneib *et al.* 1996) with five WFPC2 fields surrounding the central core. Each field was imaged at F606W (approximately rest frame V) in 12 snaps for a total of 8,400 secs. A2125 has one set of WFPC2 images centered on the brightest cluster member, 2,600 secs in F606W and 2,600 secs in F814W. In total, there are 40 objects in the A2125 field with narrow band photometry in all four filters, and 132 objects in the A2218 fields.

The WFPC2 imaging provides a rare opportunity to test our galaxy/star rejection criteria and our photometric redshift reliability. As described in our previous papers, the filter set is ‘redshifted’ so as to avoid k-corrections by providing colors in the rest frame of the cluster to be studied. The methodology of rest frame Strömgren photometry is explored in great detail in Steindling, Brosch & Rakos (2001). However, other than a comparison to cluster members with known redshifts, we have been unable to directly assess the reliability of our cluster membership criteria. The WFPC2 images will allow us to 1) determine if the object is stellar (i.e. foreground) and 2) estimate if the object is a background galaxy based on its morphological appearance (probable foreground galaxies are obvious unless near the cluster redshift).

There are 172 objects in the WFPC2 fields that were detected in all four filters. Of this sample, 29 were rejected for photometric reasons (meaning they failed the various principal component tests to determine cluster membership by photometric redshifts, see Steindling, Brosch & Rakos 2001). Inspection of the WFPC2 images finds that ten of these rejections are clearly foreground stars. Another 13 are background galaxies based on their small sizes, although we note that 1/2 of these objects are elliptical and appear to be background galaxies due to their high central surface brightnesses compared to their size (i.e. they are not dwarf galaxies). One galaxy is a foreground irregular. The remaining five have peculiar colors and/or morphologies which make it impossible to determine if they are cluster members or not. The 143 accepted objects all had morphologies that are consistent with cluster membership. There is some concern that the five peculiar objects that were rejected are cluster members and would represent a unusual cluster population for this redshift. However, it is not clear if their peculiar colors are intrinsic or due to local problems in the photometry. Repeat observations would be required to

resolve this question.

An extensive redshift survey was completed for A2218 (Ziegler *et al.* 2001). Of the 82 redshifts, five were clearly non-cluster members (four background at $z = 1.033, 0.702, 0.699$ and 0.291 , one foreground at 0.1032). The background object at 1.033 was not detected in all four filters (i.e. UV dropout) and rejected. The foreground and two other background objects were correctly rejected for anomalous colors. The remaining object, at a redshift of 0.291 , was just inside the photometric criteria, as its redshift was just outside the cluster membership limit. None of the cluster galaxies (77 galaxies) were rejected by our photometric criteria. Further inspection of the WFPC2 images indicates that rejected objects (without known redshifts) have the characteristics of background objects (i.e. small angular size and high surface brightness).

Given the information gleaned from the WFPC2 and redshift data, we believe the photometric membership criteria we have used for 20 years to be sound. High resolution WFPC2 images demonstrate that our redshifted filters correctly identify stars and eliminate them from the sample. The redshift data, although limited, indicates our procedures correctly eliminate extreme foreground and background objects, but become more problematic for galaxies with redshifts near the cluster redshifts or objects with extreme non-thermal colors (see Steindling, Brosch & Rakos 2001 for a larger discussion of this issue). The reliability of our photometric membership criteria lies somewhere between 99% (the one incorrect background galaxy by redshift) and 97% (assuming that all five peculiar galaxies are indeed cluster members).

3. DISCUSSION

3.1. Spectrophotometric Classification

The filter system used in our distant cluster studies (Rakos & Schombert 1995) is a modified Strömgren (*uvby*) system, modified in the sense that the filters are slightly narrower and the *u* filter is slightly shifted in its central wavelength as compared to the original system. The system we use herein is called the *uz, vz, bz, yz* system to differentiate it from the original *uvby* system since our filters are specific to the rest frame of the cluster that is being studied. The *uz, vz, bz, yz* system covers three regions in the near-UV and blue portion of the spectrum that make it a powerful tool for the investigation of stellar populations in SSP's (simple stellar population), such as star clusters, or composite systems, such as galaxies. The first region is longward of 4600\AA , where the influence of absorption lines is small. This is characteristic of the *bz* and *yz* filters ($\lambda_{eff} = 4675\text{\AA}$ and 5500\AA), which produce a temperature color index, $bz - yz$. The second region is a band shortward of 4600\AA , but above the Balmer discontinuity. This region is strongly influenced by metal absorption lines (i.e. Fe, CN) particularly for spectral classes F to M which dominate the contribution of light in old stellar populations. This region is exploited by the *vz* filter ($\lambda_{eff} = 4100\text{\AA}$). The third region is a band shortward of the Balmer discontinuity or below the effective limit of crowding of the Balmer absorption lines. This region is explored by the *uz* filter ($\lambda_{eff} = 3500\text{\AA}$). All the filters are sufficiently narrow (FWHM = 200\AA) to sample regions of the spectrum unique to the various physical processes of star formation and metallicity (see Rakos *et al.* 2001 for a fuller description of the color system and its behavior for varying populations).

The information that can be extracted from the narrow band colors is limited by the complexity of

a galaxy’s star formation history. For example, in passive non-starforming ellipticals, the narrow band colors can break the age-metallicity degeneracy with the caveat that the underlying stellar population are at least 5 Gyrs old with a uniform spread in internal metallicities (Rakos & Schombert 2004). Less information can be deduced from star-forming galaxies, such as spirals, in terms of their mean ages since recent star formation dominates the older stellar populations. On the other hand, the filter system does provide a convenient method of classifying galaxies based on their recent star formation rates. To this end, a spectrophotometric classification system using our filter system was outlined in Rakos, Maindl & Schombert (1996) and improved upon by the use of principal component analysis in Steindling, Brosch & Rakos (2001). For our goal of investigating cluster populations, it is beneficial to relate the photometric values to a measure of recent star formation rate rather than morphological type, although we have the expectation that these photometric classifications will map into morphological ones such that passive, red systems will typically be E/S0 types and star-forming colors will typically be late-type spirals (we will examine this hypothesis using WFPC2 images, see §3.2).

The newest form of our classification system divides the first principal component axis (PC1) into four subdivisions based on mean past star formation rate; E (passive, red objects), S (star formation rates equivalent to a normal disk galaxy), S- (transition between E and S) and S+ (starburst objects). By comparison to SED models and nearby galaxies (Rakos, Maindl & Schombert 1996), the divisions along the PC1 axis are drawn such that S galaxies correspond to those systems with spiral disk-like star formation rates (approximately $1 M_{\odot}$ per yr) and S+ galaxies correspond to starburst rates (approximately $10 M_{\odot}$ per yr). We note that since these divisions are determined by continuum colors, versus spectral lines, they do not represent the current star formation rate, but rather the mean star formation rate averaged of the last few Gyrs as reflected into the optical emission by the dominant stellar population. The red E systems display colors with no evidence of star formation in the last five Gyrs. The transition objects, S-, represents the fact that there is not sharp division between the E class and S class. These objects display slightly bluer colors (statistically) from the passive E class; however, the difference could be due to a recent, low-level burst of star formation or a later epoch of galaxy formation or an extended phase of early star formation. In addition to classification by star formation rate, we can separate out objects with signatures of non-thermal continuum (AGN) under the categories of A+, A and A- based on their PC2 values colors. It is important to remember that these classifications are based solely on the principal components as given by the color indices from four filters. While, in general, these spectrophotometric classes map into morphological ones (i.e. E types are ellipticals, S- are S0 and early-type spirals, S are late-type spirals and S+ are irregulars), this system differs from morphology by being independent of the appearance of the galaxy and based on the color of the dominant stellar population in a galaxy. This is also a classification based on integrated colors, such that large B/D galaxies (i.e. early type spirals) will generally be found in class S- as the bulge light dominates over the disk. This is in contrast to classification by morphology where the existence of even a faint disk distinguishes the galaxy from an elliptical.

The resulting population fractions based on the above photometric classifications for 153 galaxies in A2125 and 277 galaxies in A2218 are shown in Table 1. For comparison, the population fractions for the core of the Coma cluster are also shown in Table 1 (taken from Odell, Schombert & Rakos 2002). Those objects classified as non-starforming (E and S- class) comprise 74% of A2125 and A2218 compared to 95% for the core of Coma. Star-forming and starburst galaxies comprise the remaining 26% compared to only 5% in Coma. This comparison could be biased since the Coma sample is restricted

to core regions where the density-morphology relation predicts a deficiency of blue galaxies. However, analyzing the inner 500 kpc of both A2125 and A2218 (39 and 78 galaxies, listed in Table 1 as core values) yields similar fractions. These values are due to the well known Butcher-Oemler effect in these two intermediate redshift clusters (Butcher & Oemler 1978, Dressler & Gunn 1982), the increased fraction of star-forming and starburst objects compared to nearby clusters (see Pimbblet 2003 for a review). We note that, the increased number of blue galaxies is clear in both these clusters despite their different cluster morphologies, richesses and dynamical states.

3.2. Morphological Classification

The availability of HST WFPC2 images for both A2125 and A2218 in the public archive provides for a unique opportunity to compare the photometric classifications (above) with their corresponding morphological appearance and structural properties. The WFPC2 data for A2218 was obtained during the 1999/2000 observing season for HST project 7343, a gravitational lens survey. Five fields centered on the central cD galaxy were observed in F606W for 8,400 secs in each field. The WFPC2 data for A2125 was more limited, consisting of a single field centered on the brightest cluster member for 2,600 secs in F606W and F814W. For our analysis, we have co-added the F606W and F814W for increased S/N. The WFPC2 fields in A2125 and A2218 contained 168 objects (30 in A2125, 138 in A2218) with matching *uvby* photometry. Of those, 35 were rejected for photometric criteria, meaning identified by the PC analysis as either a foreground star or foreground/background galaxy.

In terms of morphology, the 137 cluster members were classified by eye as either E, S0, Sa/Sb or Sc/Irr from the WFPC2 images. This is a simplified Hubble system as outlined by Abraham (1999) where spirals are simply divided into large bulge spirals (Sa/Sb) or small bulge/irregular objects. A finer separation for spirals was deemed unnecessary given their small numbers in rich clusters. The separation of E's from S0's will depend on a noticeable disk to the galaxy, the details with respect to WFPC2 images was well studied by Ellis *et al.* (1997). When the galaxy is inclined, this is detectable as a distinct pointy edge to the isophotes versus a rounded structure (E6 in Hubble's scheme). When the galaxy is face-on, the distinction between E and S0 will depend on the visibility of a change in the light profile signaled by a lens-like feature typical to S0's. Table 2 displays the resulting matrix between spectrophotometric classification and morphology.

The morphological distribution is similar to what is seen in other intermediate redshift clusters (Dressler *et al.* 1997, Couch *et al.* 1998, Fasano *et al.* 2000) in that there is a larger number of late-type systems in A2125/A2218 as compared to present-day clusters. The A2125 and A2218 WFPC2 samples contain roughly 15% Sa to Irr type galaxies compared to 4% for Coma. There is also a shift in the fraction of ellipticals, approximately 25% of the total population in A2125 and A2218 compared to 40% in Coma. The percentage of S0's is slightly higher, 57% for A2125 and A2218 compared to 53% in Coma. These values are all in agreement with morphological estimates at similar redshifts from HST or ground-based datasets (see Fasano *et al.* 2000).

As expected, the red population in both clusters are predominantly early-type systems. Of the 37 galaxies classified by morphology as elliptical, 34 (87%) are E class photometrically, two are S- and one is classed A+ (AGN core). Of the 88 S0's, 56 (64%) are E class, 15 are S- and seven are classed as S type, where there is a statistically significant shift to bluer narrow band colors for S0's. Despite the fact

that the photometric values are integrated, only three of the ten large B/D systems (Sa/Sb) were classed as E or S- type, the rest were classed as S or S+. All the late-type systems were identified as S or S+. Thus, the relationship between spectrophotometric classification and morphology is surprisingly close to one-to-one. There is no evidence that the late-systems are ‘strangled’, meaning a sharp decrease in star formation as proposed by Couch *et al.* (2001) for A114 at $z = 0.32$, since their colors are similar to present-day spirals. However, our colors only measure the recent star formation rate, their current star formation rates (i.e. emission lines) are unknown. We also note from Table 2, that the blue population (the Butcher-Oemler population) is of a different morphological type, as well as color, compared to present-day cluster populations and, thus, there must be color and morphological evolution component to the Butcher-Oemler effect (Goto *et al.* 2003).

By morphological class, the ellipticals are the most uniform in their photometric properties and are the reddest galaxies in the sample. The S0 systems are similar to ellipticals in the range of their photometric values but more often, statistically, are classed as S- or S betraying the presence of a younger stellar population associated with their disks. Early-type spirals display the range of colors one would expect with a large bulge disk galaxy, and late-type galaxies are all classed as star-forming based on their colors. We note that the ratio of S0’s to ellipticals is approximately 2:1, similar to the ratio found in nearby clusters (Dressler 1980), although the Coma core sample has a ratio closer to 1.

3.3. Surface Photometry

In addition to classification by eye, all the objects from the WFPC2 frames were subjected to a detailed surface photometry analysis using a new automated package called ARCHANGEL (Schombert 2005). This package takes a subimage of the area surrounding the galaxy in question, determines local sky, cleans the subimage of nearby stars and galaxies, then fits a series of ellipses to the 2D intensity profile. The resulting 1D intensity profile is calibrated into a surface brightness profile using the standard HST calibration pipeline. The quality of surface photometry is generally limited by two quantities, the depth of the exposure and the flatness of the image surrounding the galaxy. The WFPC2 frames are excellent with regard to these two criteria, the exposures were long and the image quality was high such that the frames were locally flat to better than 0.5%. The extracted surface brightness profiles had typical errors of 0.1 mag arcsecs $^{-2}$ in galaxy envelopes (i.e. regions brighter than 24 mag arcsecs $^{-2}$ which was due to a combination of error along the elliptical isophote, sky error and zeropoint uncertainty. Errors increased to 0.5 mag arcsecs $^{-2}$ at a limiting surface brightnesses of 28 mag arcsecs $^{-2}$ where the fits were halted. This compares well with other surface photometry studies of cluster galaxies (Schombert 1986) and probably represents an upper boundary for WFPC2 data quality due to limitations in flatfielding. Comparison surface brightness profiles for the Coma cluster was extracted from DSS images and analyzed in an identical manner.

The resulting surface brightness profiles are then fit under the assumption that the galaxies is either a pure exponential disk, a $r^{1/4}$ shape (bulge or elliptical) or a combination of both (early-type disk galaxy with a bulge and disk). Classification by structure hopefully avoids the problem that subjective visual classification may have, especially for the E/S0 catalogories (Andreon 1998). Misclassification of an S0 as an elliptical may occur if the disk is small or very faint, however if a majority of the mass or size of a galaxy is $r^{1/4}$ then its classification as elliptical seems warrented. For the 137 galaxies in A2125

and A2218 with HST imaging, 37 (27%) are $r^{1/4}$ shaped, 27 (20%) are pure exponential disks and the remaining 73 (53%) are bulge+disk objects (see Table 3). This distribution by profile type differs significantly from the distribution found in the Coma sample where 43% of the galaxies are $r^{1/4}$ shaped, 36% are pure exponential disks and 20% are bulge+disk objects. The difference between the Coma and A2125/A2218 samples being primarily due to the increase in $r^{1/4}$ shaped objects (ellipticals) and the decrease in bulge+disk objects (S0's and early-type spirals) relative to Coma. The blue population (S/S+) in A2125 and A2218 are mostly disk systems (17 out of 27, the remain 10 are bulge+disk objects).

Both clusters display a ratio of S0's to ellipticals near two (under the assumption that all red $r^{1/4}$ objects are ellipticals and all red B+D or D objects are S0's), which is similar to the value determined for nearby clusters by Dressler (1980). But, a HST survey of ten clusters between $z = 0.3$ and 0.6 (Dressler *et al.* 1997) finds the S0 to elliptical ratio to be approximately one by redshifts of 0.3 (although we note that Fabricant, Franx & van Dokkum (2000) find a ratio of 1.6 for CL1358+62 at $z = 0.33$ which is more in agreement with our values). Our S0 fractions (approximately 55%) for A2125 and A2218 agrees well with the measured morphological trends of 25 clusters ranging from $z = 0$ to 0.6 by Fasano *et al.* (2000) (see their Figure 9), but our elliptical fraction of 25% is slightly below their values of 30% to 35% at redshifts of 0.2. This difference may be due to subtle differences in visual morphology versus surface photometry (Andreon 1998), but the structural differences between ellipticals and S0's were clear to visual inspection if detectable in their surface brightness profiles.

Comparing visual morphology to surface brightness structure (Table 4), we find that a majority of the morphologically classified S0 galaxies in A2125 and A2218 are composed of a bulge plus disk (B+D) structure. In contrast, Coma S0's are mostly pure disk systems (lenticulars under the nomenclature proposed by van den Bergh 1990). The distinction between B+D S0's and lenticulars (disk only) is not an artifact of the fitting process. Figure 1 displays a mosaic of two B+D S0's and two lenticulars from A2218. The left panels are low contrast images to emphasize the inner bulge regions, the right panels are high contrast images to emphasize the outer disk. It is clear from this Figure that B+D S0's have a separate, round bulge region with a distinct and flattened disk. The lenticulars have no break in their profile to signal a bulge, nor any change in flattening of the inner isophotes.

The fact that S0 galaxies divide into two populations by structure has been previously noted before in an analysis of the RSA (van den Bergh 1994). In that study, a comparison is made between the colors and luminosity functions of E's, S0's and Sa's where the S0 population is found to be intermediate in color and gas/dust content between E's and Sa's, however, their absolute luminosity has a lower mean value than either E's or Sa's. Comparing the structure of galaxies in our Coma sample, we find that the S0's in the core of Coma are also composed of a dual population, where the brighter S0's are the B+D objects and the fainter S0's are lenticulars. This is the same distinction that is found in the A2125 and A2218, where the S0 galaxies neatly divide into the bright objects (bulge+disk) and the fainter lenticulars (disk only). However, when we compare the population fractions in A2125/A2218 to the Coma core sample, Coma is deficient in the bright S0's and the total Coma S0 population has a mean luminosity that is 1.5 mags fainter than the combined A2125/A2218 S0 population.

One explanation for the change in the S0 population (from B+D dominant to lenticular dominant) is that S0 disks fade (or are destroyed) on the short cosmological time from $z = 0.2$ such that past B+D S0's now appear as a pure $r^{1/4}$ ellipticals today. This can be tested by examining the correlations of the

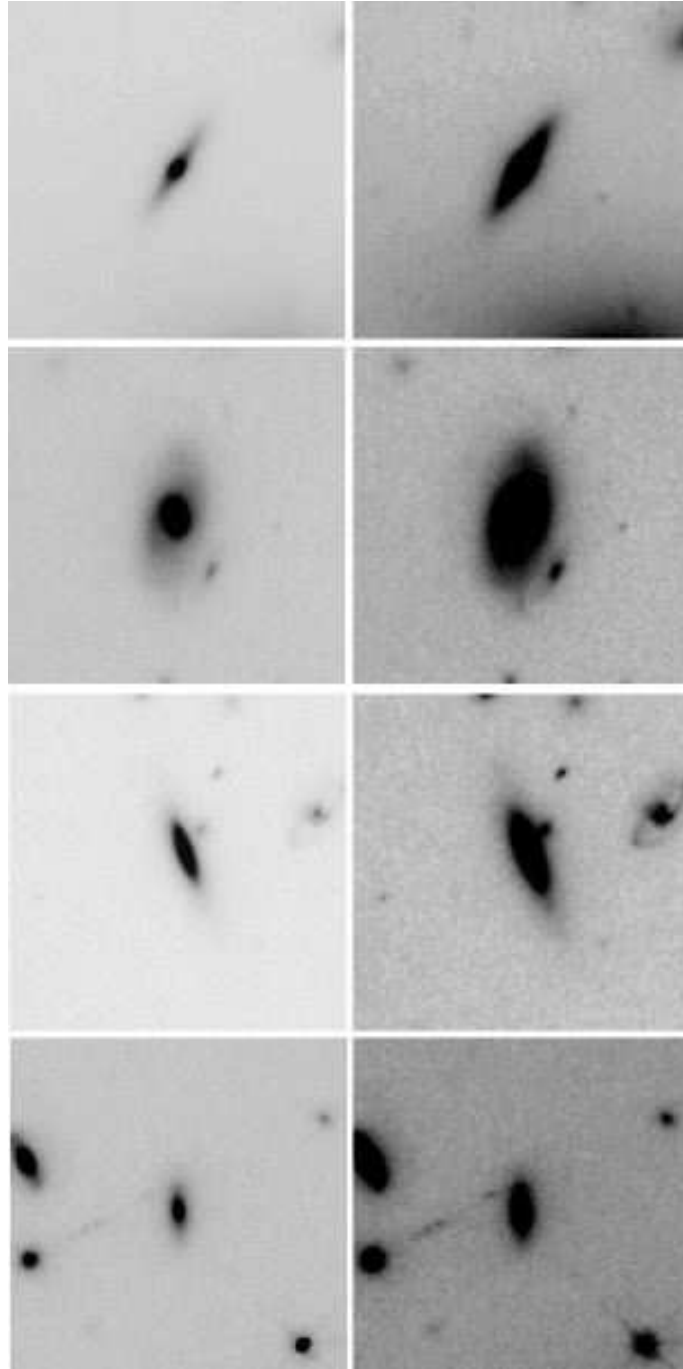


Fig. 1.— The above figure is a mosaic of four S0 galaxies in A2218, two classical S0's and two lenticulars. The left hand panels are of low contrast to emphasize the core regions. The right hand panels are of high contrast to display the outer isophotes. The top two galaxies are bulge+disk systems (B+D), meaning they have distinct bulge and disk components in their surface brightness profiles. The bottom two galaxies are pure disk systems (lenticulars). The differences in their inner structure is clear in the low contrast images, while their visual morphology is similar. A2125 and A2218 are unusual (compared to Coma) by having a high fraction of B+D S0's compared to lenticulars.

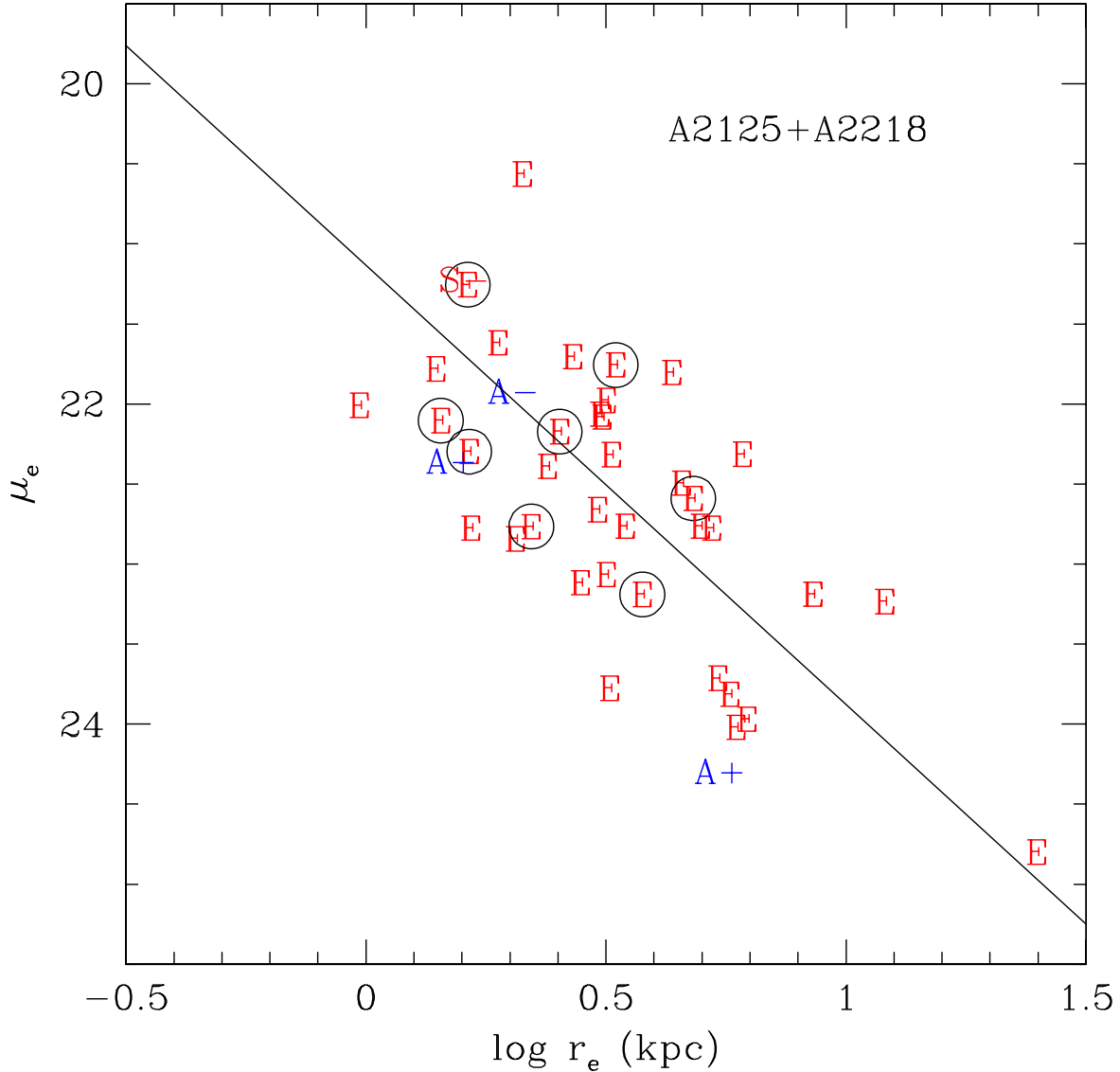


Fig. 2.— The $r^{1/4}$ structural parameters effective radius (r_e) versus effective surface brightness (μ_e) for all bulges ($B/D > 0.1$) and elliptical shaped objects in the WFPC2 fields for A2125 and A2218. Symbols display the galaxy's photometric classification. Circled symbols are B+D S0's. The solid line is the relation for ellipticals from Kormendy (1980) corrected for surface brightness dimming at the mean redshift of A2125 and A2218. Galaxies in both clusters with $r^{1/4}$ profiles (ellipticals and S0 bulges) follow the same structural relation as present-day ellipticals.

structural parameters derived from the surface photometry. Ellipticals and S0 bulges, described by an $r^{1/4}$ shape, are parameterized by the effective surface brightness (μ_e) and effective radius (r_e). These two values are shown in Figure 2 where each galaxy is represented by its photometric classification. For clarity, only pure $r^{1/4}$ and large bulge ($B/D > 0.1$) galaxies are shown as small bulge fits suffered from numerical errors due to the dominance of the disk intensity. For comparison, the solid line is from Kormendy (1980) converted to the Benchmark cosmology and corrected for surface brightness dimming (there are no k-corrections since F606W is equivalent to rest-frame V at these redshifts). Despite the lookback time to A2125 and A2218, their $r^{1/4}$ structural correlations are identical to present-day galaxies. The scatter about the Kormendy relation is similar to that of other bright cluster ellipticals (see Figure 6, Schombert 1986). The circled data points represent large S0 bulges which follow the same relationship as the ellipticals, meaning that if these S0's were stripped of their disks, they would have the same structural properties as present-day cluster ellipticals.

Disk structural parameters are more difficult to interpret as there is no clear scale length to characteristic surface brightness relation as is found for ellipticals. This lack of correlation between scale length and surface brightness is due to the wide range in past star formation rates and formation processes in spirals which reflects into a range of central surface brightnesses. Despite varying star formation histories, there is a trend of increasing central surface brightness for early-type spirals. The most recent study of the disk structure of spirals is MacArthur *et al.* (2004). Taking a straight line through their brightest spirals (see their Figure 1), produces the line shown in Figure 3 (corrected for the distance to A2218). Compared to this relationship, most of the blue disk galaxies in A2125 and A2218 have similar central surface brightnesses as the typical spiral from MacArthur *et al.* . On the other hand, many of the red disks (S0's) are fainter than the MacArthur *et al.* relation. This suggests a connection between the lack of lenticular S0's in Coma in the sense that these systems in A2125 and A2218 are faded compared to their present-day counterparts and, perhaps, are ‘missing’ in the Coma sample simply because they have converted into elliptical shaped galaxies with invisible (with respect to surface brightness) disks. In addition, if stellar luminosity traces mass, then the mass density of these disks is low and they are susceptible to stripping by the cluster tidal field.

3.4. Multi-color Diagrams

Our primary diagnostic for understanding the colors of cluster galaxies is the multi-color diagrams $uz - yz, bz - yz, vz - yz, bz - yz$ and $vz - yz, mz$. Figures 4 and 5 display these multi-color diagrams for all the detected galaxies in A2125 (153 galaxies) and A2218 (277 galaxies). All galaxies classified as E or S- are marked in red, classes S and S+ (as well as A) are marked in blue. The size of the symbol indicates the galaxy's absolute magnitude. In general, the multi-color data for A2125 and A2218 follows the trends for other intermediate redshift rich clusters (Rakos & Schombert 1995). Like present-day clusters (i.e. Coma), a majority of the galaxies have red, passive colors usually associated with elliptical and S0 morphologies. Unlike nearby rich clusters, there are a large number of blue, star-forming or starburst systems in each cluster (the Butcher-Oemler effect). The red population has a relatively tight grouping in each diagram, the correlation between various colors reflects the differences in metallicity with galaxy mass (see below). Each cluster's blue population is distinct from the red population. A2125 differs from A2218 in having a grouping of very bright blue galaxies around $bz - yz = 0.1$ and $vz - yz = 0.0$ (see discussion of color-magnitude diagram below).

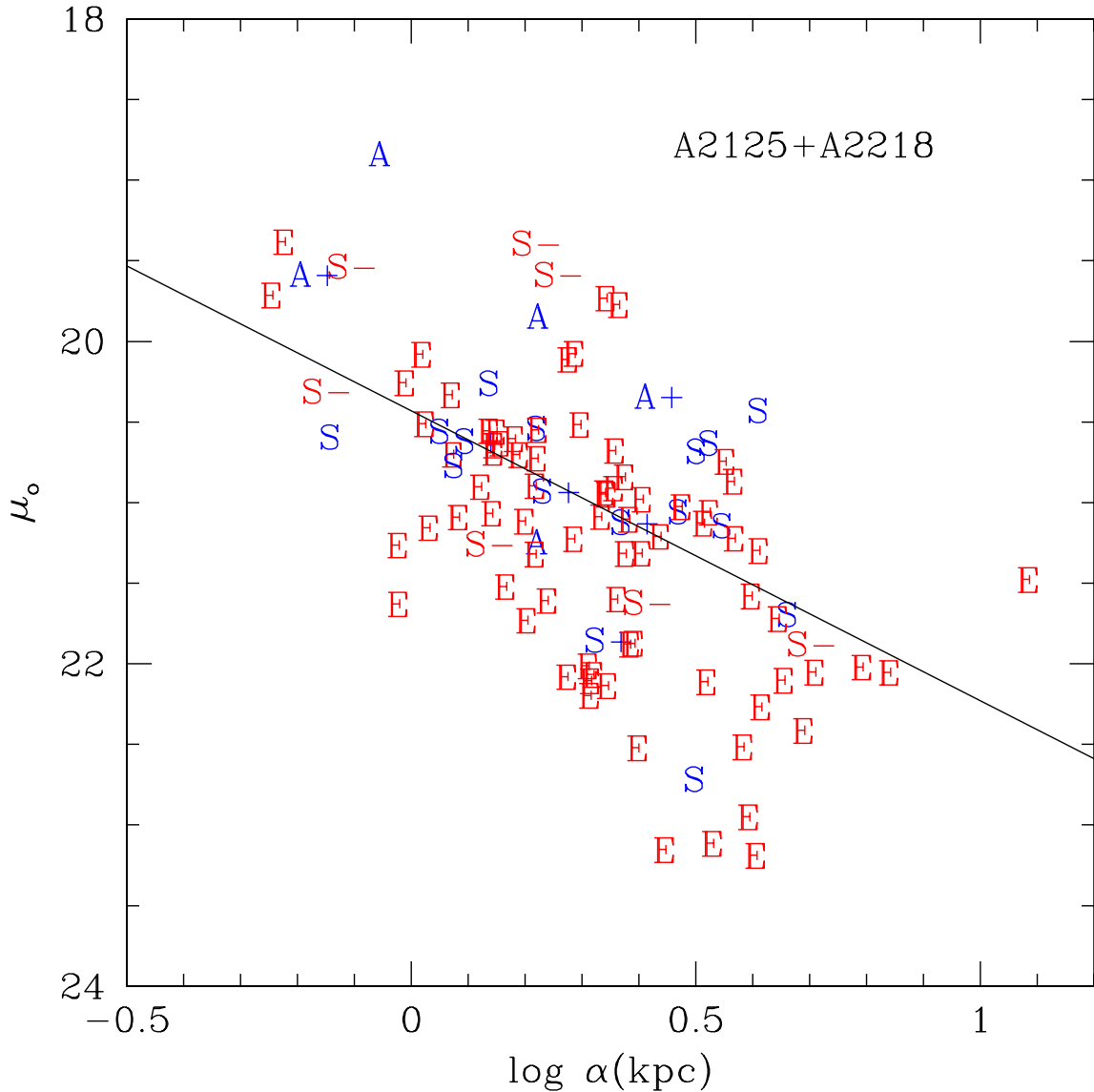


Fig. 3.— The disk scale length (α) versus the disk central surface brightness for all the B+D and D type galaxies in A2125 and A2218. Symbols display the galaxy's photometric classification. The solid line is from MacArthur *et al.* (2004) and represents the mean relation between central surface brightness and scale length for a range of Hubble classes. The blue population follows the MacArthur *et al.* relation (higher central surface brightness due to ongoing star formation). A majority of the systems below the solid line are S0's with faded disks.

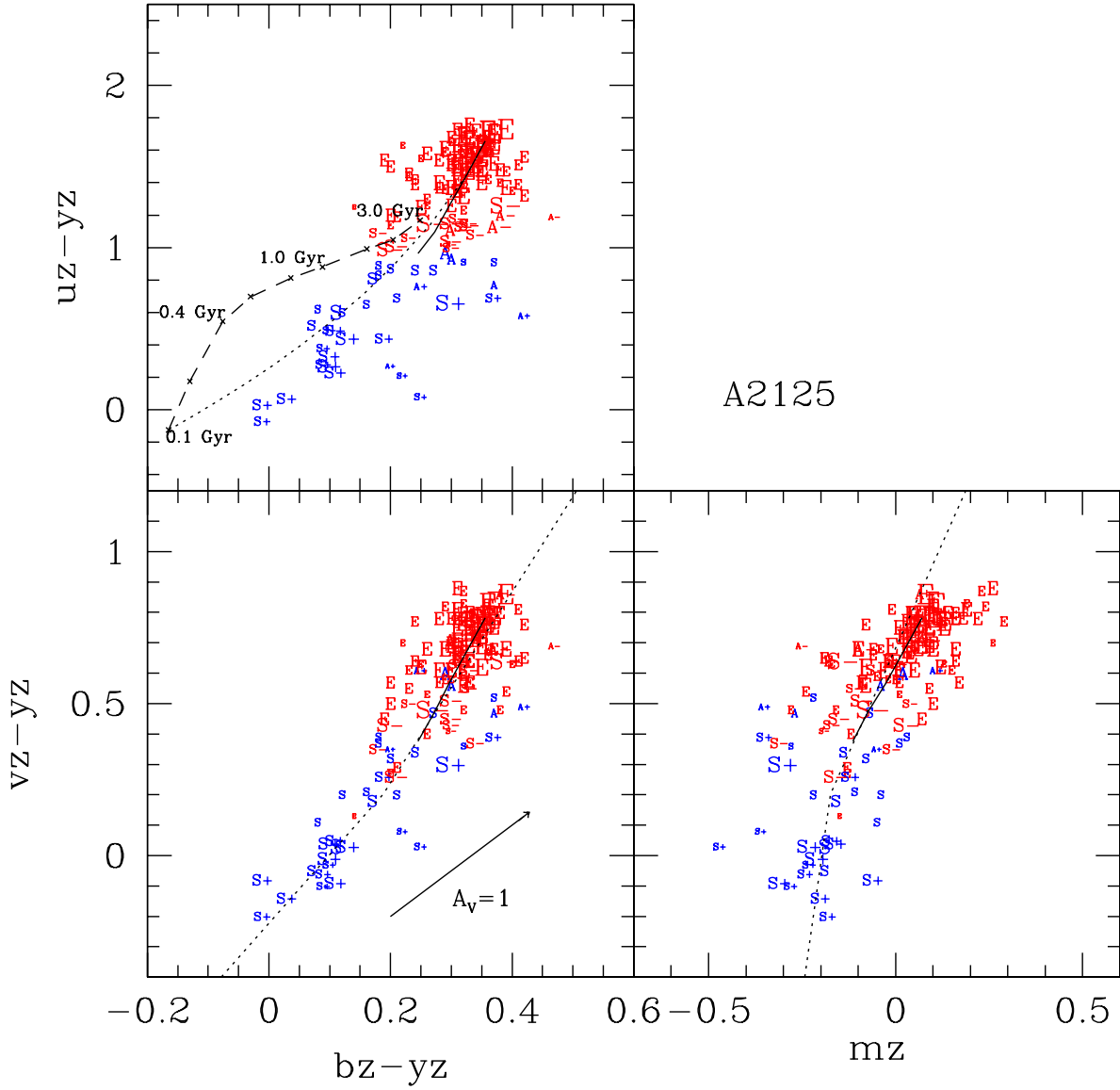


Fig. 4.— Multi-color diagrams for A2125. All three colors and the mz index are shown for galaxies determined to be cluster members by photometric criteria. Photometric classification is shown by symbol type (E, S-, S, S+) and the red population is denoted by that color as is the blue population. Symbol size indicates absolute luminosity of the object. The solid line in each diagram displays the 13 Gyr models for metallicities ranging from -0.7 to $+0.4$. The dotted line in the $vz - yz$ and mz diagrams represents the 99,000 galaxies from the SDSS sample (Smolcic *et al.* 2004). The dashed line in the $uz - yz$ diagram is the range in age for a solar metallicity model. The dotted line in the same diagram displays a ‘frosting’ model, i.e. adding increasing fractions of a 0.1 Gyr population to a 13 Gyr population. A reddening vector is shown in the $vz - yz$ diagram.

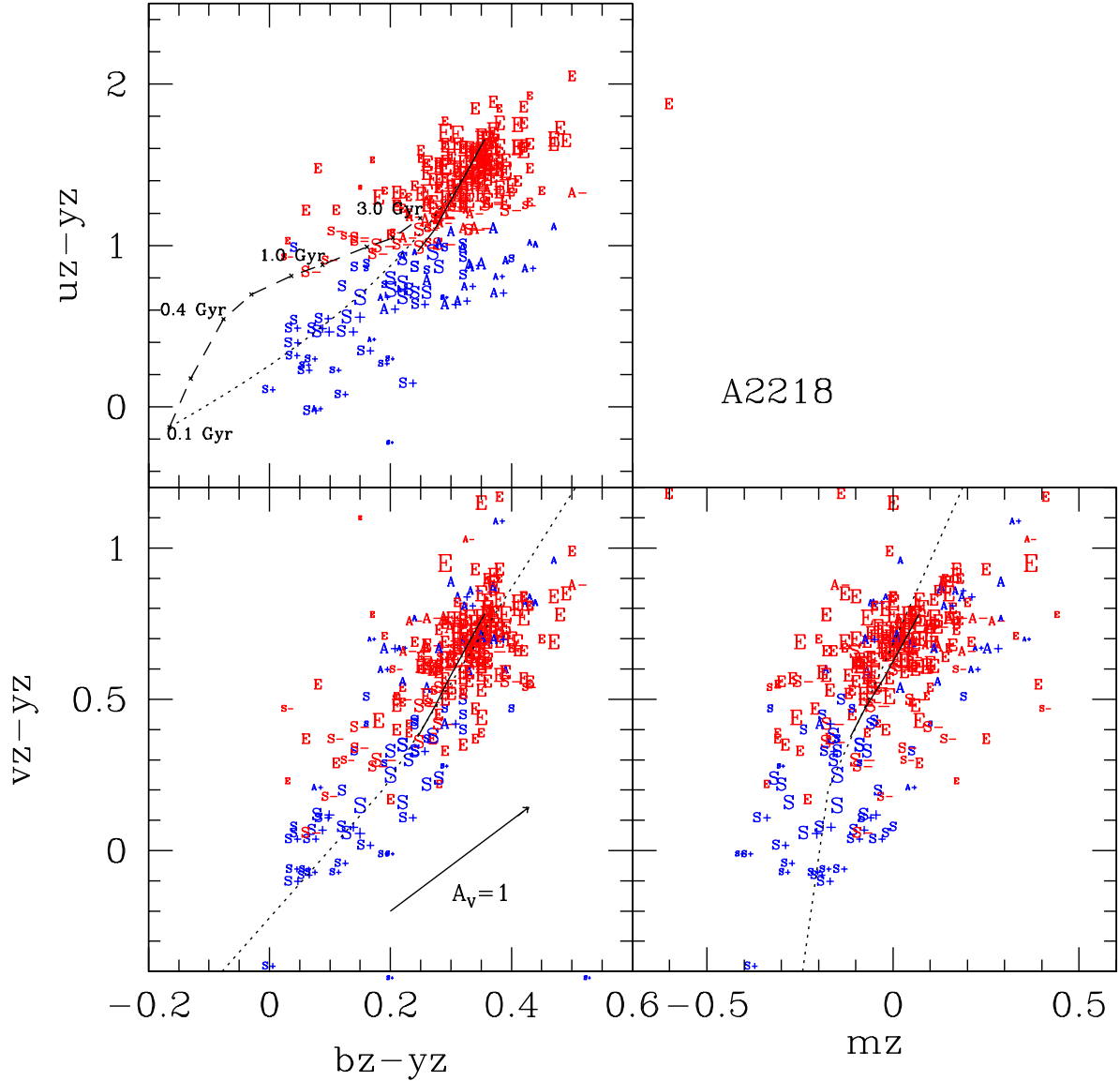


Fig. 5.— Multi-color diagrams for A2218. Symbols and lines are the same as Figure 4.

The dotted lines in $vz - yz, bz - yz$ and $vz - yz, mz$ diagrams are the mean color track of 99,000 SDSS galaxies (Smolcic *et al.* 2004). These colors were extracted from a flux limited sample of SDSS spectra (which does not cover the uz filter), converted to rest frame. The scatter about this locus is 0.03 mags. Both clusters track the same locus, although with more scatter reflecting the lower S/N data of our sample. Also indicated in the diagrams are a series of SED models taken from Bruzual & Charlot (2003) and convolved to our multi-metallicity models (see Rakos *et al.* 2001). The solid line in all three panels displays the run of color for a 13 Gyrs population with mean metallicities ranging from $\text{Fe/H} = -0.8$ to $+0.4$ (blue to red). The red galaxies in our sample (classes E and S-) nicely bracket the 13 Gyrs models. The dashed line in the $uz - yz$ panel is a run of pure age populations of solar metallicity ranging from 0.1 Gyr to 3 Gyrs old. Even the bluest galaxies in our sample fail to match a pure young population indicating the presence of an old stellar population in all cluster galaxies. The dotted line in the same panel displays the fractional mixture of a 0.1 Gyr population and a 13 Gyrs population, so-called ‘frosting’ models. The blue galaxy population colors are well matched to this type of model indicating that even starburst galaxies have a significant underlying older population in their integrated colors.

Galaxies composed of a single aged and old stellar population will form a linear sequence in this diagram with position being determined solely by the mean metallicity of the underlying stars. Since these are integrated colors, the metallicity reflected by the color is a luminosity weighted value (versus spectroscopic values which are surface brightness weighted and usually represent core values). Based on our metallicity calibration from globular clusters (Rakos & Schombert 2005), the galaxies with the reddest colors have mean metallicities just above solar, dropping to values of $[\text{Fe/H}]$ between -0.5 and -1.0 for the galaxies a magnitude fainter than L_* . In our previous work, we have demonstrated an age dependence for ellipticals (E class) with luminosity (Odell, Schombert & Rakos 2002), but this effect is minor in the $vz - yz, bz - yz$ diagram compared to metallicity effects. While star-forming galaxies appear to follow the same linear relation in Figures 4 and 5, in fact their colors are dominated by a number of young, massive stars and not metallicity effects. In addition, several S and S+ class objects lie below the sequence of ellipticals along the extinction vector from their bluer counterparts indicating the presence of dust.

The $vz - yz, mz$ diagram ($mz = (vz - bz) - (bz - yz)$) is used to separate systems with a history of moderate to strong star formation from those with passive histories (ellipticals), and also to distinguish non-thermal colors (AGN’s) from stellar colors. The photometric classification is best done with PC analysis (which uses all the color information, see Steindling, Brosch & Rakos 2001), although one can see that almost all star-forming galaxies have low mz values. The information in this diagram is further confused as one samples deeper into a cluster’s luminosity function. Faint dwarf ellipticals ($M_{5500} > -17$) have low mz values due to a combination of extreme old age and low metallicity (see Rakos & Schombert 2003). However, this is not a concern for this study since we limit ourselves to galaxies with M_{5500} brighter than -18 .

The $uz - yz, bz - yz$ diagram is a measure of recent star formation rate. Even objects with non-thermal colors easily separate from passive red objects in this diagram since the amount of UV light is directly proportional to the number of massive stars, aside from extinction effects. Comparison with SED models indicates that galaxies with $uz - yz$ values between 0.7 and 1.0 have mean star formation rates (over the last 0.5 Gyrs) similar to spiral disks (i.e. $1-2 M_\odot/\text{yr}$, assuming near solar mean metallicities). Galaxies with $uz - yz$ values below 0.7 are undergoing a starburst with SFR at,

or greater than, $10 M_{\odot}/\text{yr}$. A majority of the star-forming galaxies in both A2125 and A2218 display $uz - yz$ colors in agreement with the ‘frosting models’, i.e. an older population undergoing a recent burst of star formation. The remaining blue galaxies appear to be star-forming colors with medium extinction values (A_V between 0.5 and 1.5).

3.5. Color-Magnitude Relation

The color-magnitude diagram for ellipticals is the most common tool for investigating red populations in clusters and is considered to be a classic demonstration of the varying metallicity with galaxy mass for old cluster populations. Discovered in the days of photoelectric photometry (Faber 1973, Visvanathan & Sandage 1977), the color-magnitude relation (CMR) is typically interpreted as the increasing ability for deeper gravitational wells (higher luminosity systems) to maintain a chemically enriched ISM (Larson 1974, Arimoto & Yoshii 1987). Early CMR’s were observed in near-blue colors, such as $U - V$, however, since then the CMR has been investigated from the far-UV to the near-IR (Pahre 1999, Ellis *et al.* 1997). With respect to the $uvby$ filter system, we have previously presented a full analysis of our filter system’s behavior with galaxy luminosity in Coma and Fornax (Odell, Schombert & Rakos 2002).

While the color-magnitude relation has been studied at many wavelengths (Pahre 1999) and spectroscopically, using line indices and velocity dispersions in the place of color and luminosity (Kuntschner 2000, Trager *et al.* 2000), there is no theoretical expectation that the relationship should be a linear or tightly constrained. In other words, the star formation history of galaxies can be diverse and there is no reason why the CMR should exist nor why its scatter is so small (Andreton 2003). Mean stellar age can have a strong effect on the CMR, but from analysis of galaxy color and line indices (Kuntschner 2000, Trager *et al.* 2000) and due to a lack of visible change in the CMR with redshift (Stanford, Eisenhardt & Dickinson 1998), it is generally accepted that the CMR reflects a mass-metallicity sequence in an old stellar population. The low scatter to the CMR, in what is apparently a solely metallicity effect, is interpreted to mean that the formation of ellipticals is coeval and uniform (the so-called monolithic model of galaxy formation, see Andreton 2003 and Ellis *et al.* 1997 for a review). Hierarchical models of galaxy formation (Kauffmann & Charlot 1998) can reproduce the CMR, but the low scatter makes the process highly contrived.

The color-magnitude relation for A2125 and A2218 is shown in Figures 6 and 7, where the top panel displays the near-UV color, $uz - yz$, the middle panel displays the metallicity color, $vz - yz$, and the bottom panel displays the continuum color, $bz - yz$, as a function of M_{5500} . The solid lines are fits to the color-magnitude relation for Coma with the dotted lines in $vz - yz$ displaying the 3σ variation to the Coma fit (note, these fits were made only to those systems which were morphologically classified as ellipticals in Coma, see Odell, Schombert & Rakos 2002). While our discussion below will be confined to the photometric E class objects, all the cluster data from E to S+ are shown for completeness.

The $uz - yz$ CMR diagram is nearly equivalent to $U - V$ based on central filter wavelength, although the $uz - yz$ color samples a much narrower portion of a galaxy’s SED. While the uz region of the spectrum is sensitive to metallicity effects, it is much more sensitive to light from hot, massive stars, i.e. recent star formation and mean age. Yet, the correlation between luminosity and color is the strongest, and with the lowest scatter, in the $uz - yz$ colors. Luminosity and $vz - yz$ color is also well

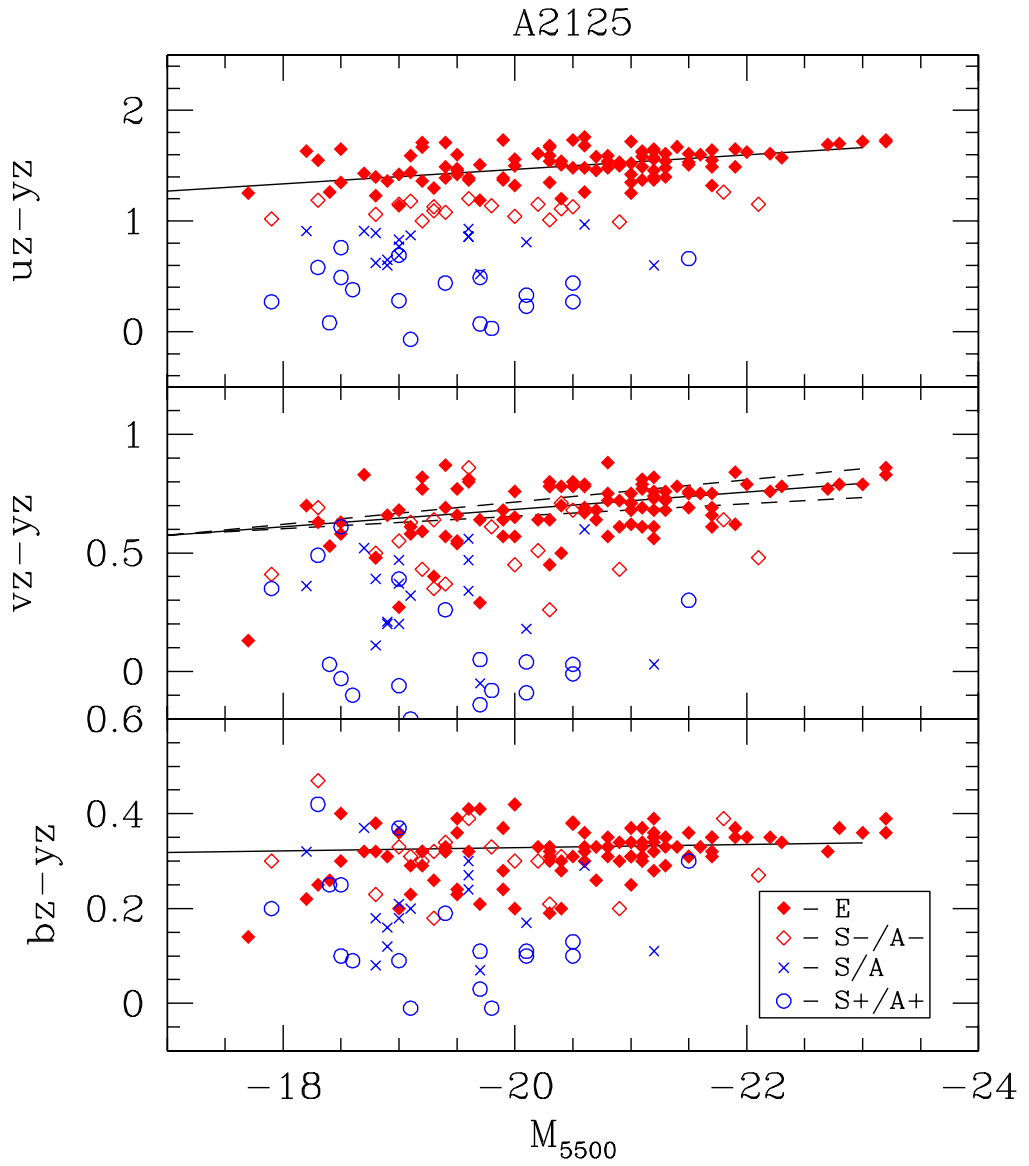


Fig. 6.— The color-magnitude diagram in three colors for A2125. Symbol types for the different photometric classifications are shown. The red population (class E and S-) are shown in red, the blue population (S and S+) are shown in blue. The solid line is the fit to the Coma/Fornax data from Odell, Schombert & Rakos (2002), dashed lines in the $v_z - y_z$ diagram display the 3σ errors on the fit. The similarity to Coma is striking, even reproducing the flat $b_z - y_z$ relation which is unexpected in Coma, or this paper’s data, as metallicity effects should be detectable in the $b_z - y_z$ color. A lack of slope indicates a competing age effect such that lower mass galaxies are older.

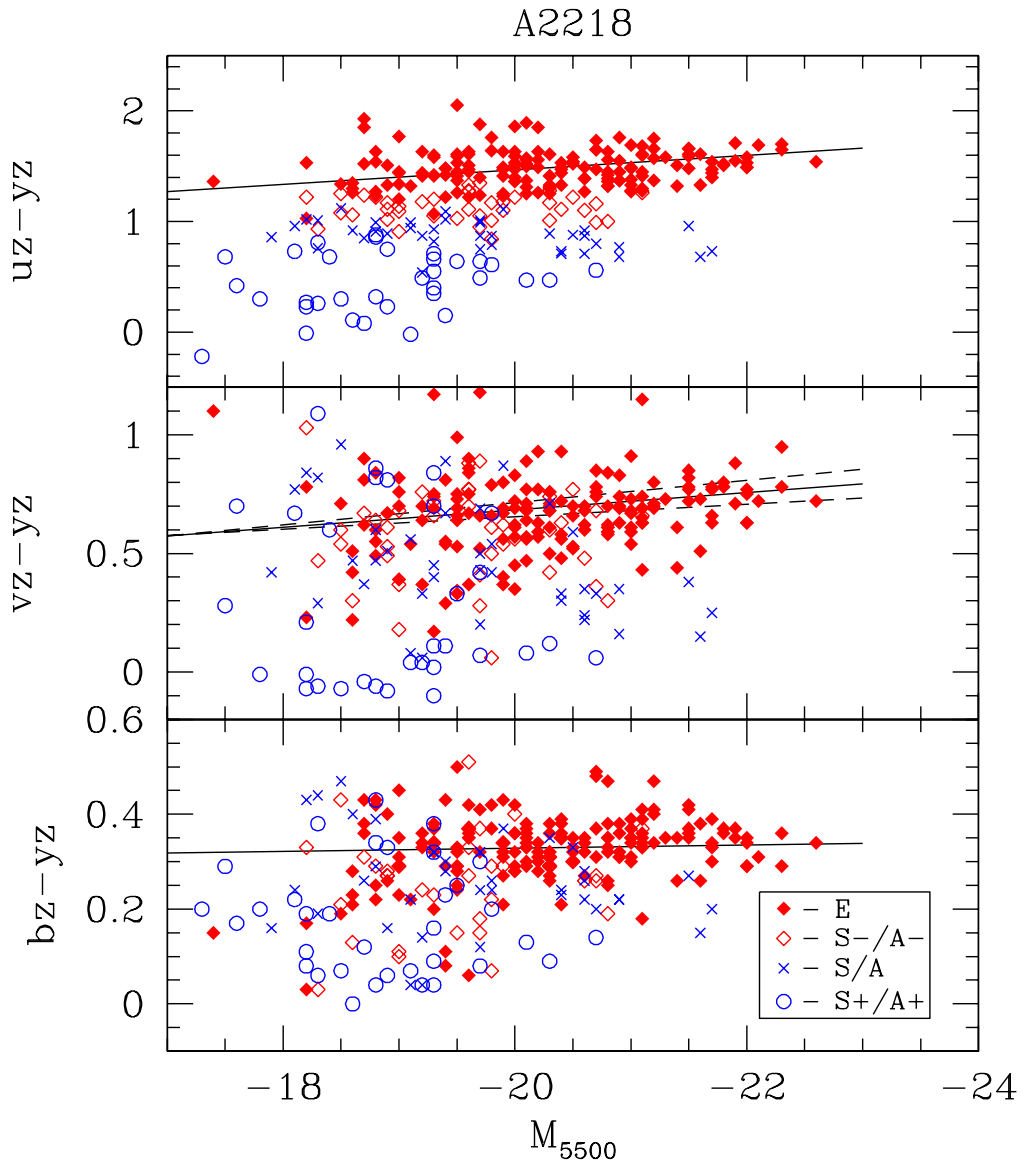


Fig. 7.— The color-magnitude diagram in three colors for A2218. The symbols and lines are the same as Figure 6.

correlated, in agreement with the expectation that $vz - yz$ is a strong metallicity indicator. However, the relation for $bz - yz$ is much weaker, although in agreement with Coma $bz - yz$ data. In all three diagrams, the scatter around the Coma fits is larger than observational error.

If the CMR is reflecting a mass-metallicity relationship, then interpretation requires converted luminosity to mass and color to [Fe/H]. Conversion of luminosity to mass requires a calibration of M/L , which for ellipticals is narrow and linear (Bender, Burstein & Faber 1992). Relating the color axis to metallicity is more problematic. Our initial calibration of $vz - yz$ to [Fe/H] was through the use of globular cluster colors and spectroscopic [Fe/H] values. However, globular clusters are single metallicity plus single age systems and galaxies must be composed of a range of stellar populations with varying metallicities and, possibly, varying age. While a multi-metallicity population is relatively easy to calculate from globular cluster colors, a varying age population is not due to the lack of a range on ages in globular cluster system around the Milky Way. For this reason, we have adopted a system of globular cluster metallicities to calibrate models of simple stellar populations (SSP's, see Schulz *et al.* 2002), and then using these models to explore age variation.

Our technique for calibrating the $vz - yz$ to [Fe/H] is outlined in Rakos & Schombert (2004). From these empirical calibrations, we extend the metallicity scale to a range of SSP's available in the literature, then construct a model for a single galaxy as the sum of a Lorenzian distribution of metallicities where the peak [Fe/H] value is a free parameter and a corresponding long tail towards low [Fe/H] values. Each metallicity bin has a corresponding population color which is summed by luminosity weight. Each galaxy is characterized by a mean metallicity ($\langle \text{Fe/H} \rangle$), a numerical mean of the total population as weighted by luminosity (this value is always slightly less than the peak metallicity, which is more typical of spectroscopic values taken from the bright, metal-rich core regions of galaxies). The resulting multi-metallicity models explain all the details of the $\langle \text{Fe/H} \rangle$ versus $vz - yz$ diagram determined from spectroscopic [Fe/H] values (see Rakos *et al.* 2001).

Armed with this calibration method, we find that $vz - yz$ colors near 0.75 correspond to $\langle \text{Fe/H} \rangle$ values of +0.2 for the high luminosity galaxies in A2125 and A2218. Likewise, $vz - yz$ colors of 0.60 for low luminosity galaxies corresponds to $\langle \text{Fe/H} \rangle$ values of -0.5 (these axis are shown in Figure 9 to be discussed below). Of course, it is naive to expect that each galaxy arrives at its final metallicity based solely on mass given the numerous environmental processes that occur in rich clusters. However, the linear nature of the color-magnitude (in a log-log parameter space) does imply that a coherent process is in operation for the stellar populations in elliptical galaxies, if their point of origin extends to redshifts greater than 5.

While it is universally accepted that a majority of the CMR is due to metallicity, age effects can play an important component. In fact, one of the key differences between the monolithic scenarios of elliptical formation (Eggen *et al.* 1962) and the hierarchical model (Kauffmann 1996) is the role that age will play. Monolithic formation implies a very narrow range of age within an ellipticals stellar population, whereas hierarchical formation could result in a narrow range if all the component galaxies have single formation epochs or a range in age if the merging components have varying formation epochs (Kauffmann & Charlot 1998).

Observationally determining an age difference is a difficult task even for narrow band filters due to the age-metallicity degeneracy. For galaxies with old stellar populations, the two color diagram in Figures 4 and 5 can resolve age differences between 2 to 3 Gyrs (see Rakos & Schombert 2004) with

the caveat that the dominant stellar population in the galaxy in question is older than 5 Gyrs and has not undergone a recent star formation event or absorbed a younger stellar population. A younger mean age displays itself through the continuum color, $bz - yz$. According to expectations from our multi-metallicity models, and the observed slope of CMR for $vz - yz$, we find there should be a shallow, but measurable slope in $bz - yz$ with luminosity. However, analysis of the $bz - yz$ colors in both A2125 and A2218 (and Coma plus Fornax) indicates zero slope in $bz - yz$ versus luminosity, even though the metallicity changes a full dex for the luminosity range. The most obvious interpretation is a competing age effect in the direction such that lower mass galaxies are older. While, to first order, this appears to be a stunning victory for the hierarchical scenarios (dwarf galaxies formed first and more massive systems are constructed from a combination of old dwarfs and spirals), in fact, this trend could be derived in many ways. For example, bright ellipticals in rich clusters clearly have a history of mergers and the cannibalism of even one star-forming spiral or irregular would push their continuum colors bluer and force an underestimation of their mean ages. This interpretation also draws some support from the fact that the scatter of the brightest galaxies in the $bz - yz$ CMR is greater than any other color, which is predicted for a random process such as mergers.

The morphological information from the WFPC2 images allows us to inspect the CMR for differences between ellipticals and S0's since the claim is made, based on spectroscopic measurements of Coma galaxies, that a significant fraction of S0's have undergone star formation in the last 5 Gyrs (Poggianti *et al.* 2001). This is a key statement concerning the star formation history of galaxies based solely on their morphology appearance and, in this case, the existence of a disk implies an extended phase of star formation. There are 112 galaxies in the WFPC2 fields of A2125 and A2218 with morphological classifications of E (36 galaxies) or S0 (76 galaxies). A comparison of their colors over a range of luminosities will be biased due to the CMR. To avoid this effect, we have examined a histogram of the differences from the $uz - yz$ CMR for each galaxy type. Figure 8 displays the resulting histogram and it is clear that the ellipticals form a well shaped gaussian around the zeropoint, but that S0's have a slightly different mean value and a long blue tail. This confirms the Smail *et al.* (2001) result that S0's display slightly bluer integrated colors (in a range of optical and near-IR colors) consistent with a prolonged period of star formation as compared to ellipticals (for a dissenting view, see Jones, Smail & Couch 2000). We note that Ziegler *et al.* (2001) find no difference in age between the ellipticals and S0's in A2218, although theirs was a spectroscopic study (i.e. galaxy core values) for a small sample in the very center of A2218. Thus, it may be true that S0 bulges and ellipticals have a similar age and if S0's have a prolonged episode of star formation, the evidence for this epoch will most likely be in their disks and not their galaxy cores. A difference of 0.2 mags in $uz - yz$ in Figure 8 would correspond to color change from a 5 Gyrs population to a 13 Gyrs population (assuming that this color represents the total luminosity of the galaxy of roughly solar metallicity), which corresponds well with the Poggianti *et al.* estimate of 5 Gyrs minus 2 Gyrs of lookback time.

3.6. Color Evolution of the Red Population

The relatively low scatter in the $vz - yz$ CMR at high luminosities (Andreon 2003), and its consistent slope from cluster to cluster (Bower *et al.* 1992, Aragon-Salamanca *et al.* 1993, Ellis *et al.* 1997, Stanford, Eisenhardt & Dickinson 1998, Kodama *et al.* 1998), presents an opportunity to examine very small color differences in the red population due to lookback time, i.e. color evolution. Higher

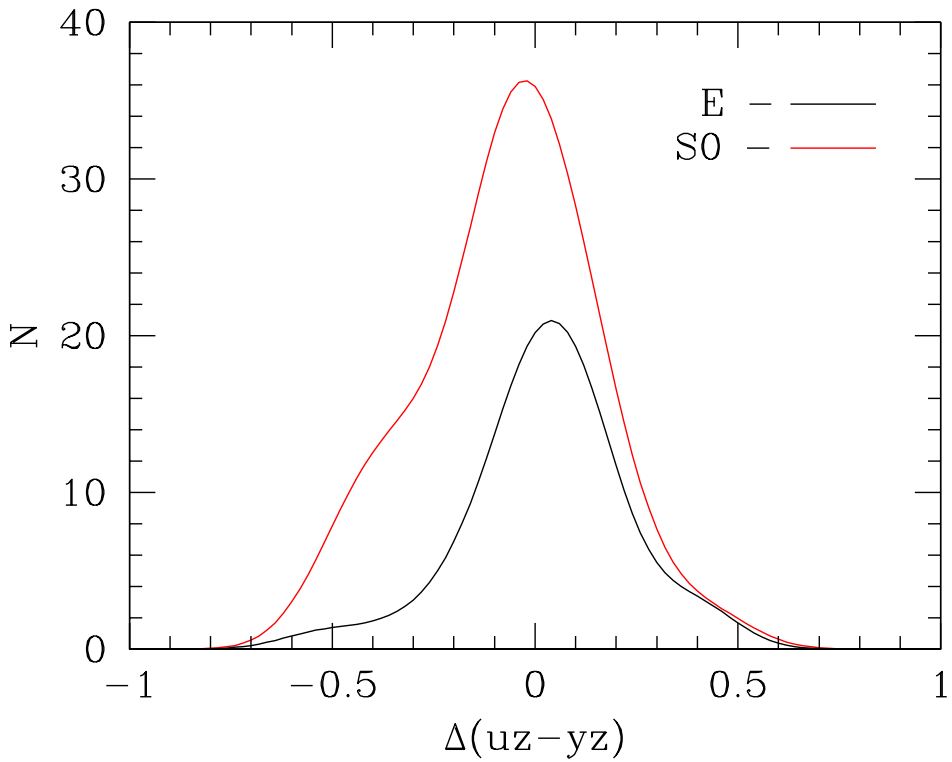


Fig. 8.— Normalized histogram of the difference in the $uz - yz$ colors as measured from the mean CMR line for morphologically determined ellipticals and S0's. The ellipticals in A2125 and A2218 display a mean of zero around the CMR; whereas the S0's from the WFPC2 sample have a clear tail to the blue. Since $uz - yz$ measures recent star formation, when corrected for metallicity effects of the CMR, then the blue tail indicates a younger mean age for S0's or a recent episode of star formation. A shift of 0.2 in $uz - yz$ color occurs between a 5 Gyrs and 13 Gyrs population. Thus, either S0's had their last star formation 5 Gyrs ago, or have experienced a more recent episode involving some small fraction of the total stellar population on top of a 13 Gyrs population.

redshift clusters also offer the advantage of higher richnesses (meaning more data) at the bright end of the CMR. For example, the number of galaxies brighter than $M_{5500} = -20$ in A2218 is about three times the number in Coma. A2218 is at a redshift of 0.175 and A2125 is at a redshift of 0.247 which corresponds to a lookback times of 2.0 and 2.7 Gyrs ($H_0 = 75 \text{ km sec}^{-1} \text{ Mpc}^{-1}$, $\Omega_m = 0.3$, $\Omega_\Lambda = 0.7$). The Bruzual and Charlot (2003) spectrophotometric models, convolved to our multi-metallicity scheme, predict a change in $vz - yz$ of 0.03 (blueward) and a increase in luminosity of 0.21 mags for a time interval of 2.5 Gyrs (assuming that present day ellipticals in Coma are 13 Gyrs in mean stellar age).

In previous papers, our analysis technique at this point was to ignore the changes in luminosity and focus on the mean color of the red population. This requires setting a limiting magnitude to the sample, since fainter galaxies are bluer, and adopting a cutoff criteria to divide the blue and red populations. While the mean color is a robust measure of the red population, the combined effects of color selected samples, bias at the limiting magnitude and the CMR itself limit its usefulness. With a sufficient number of galaxies, and a better classification procedure, it should be possible to divide the red population into magnitude bins and compare the CMR from averaged colors to the model predictions.

Figure 9 presents just such an analysis for the red populations in A2125 and A2218 (combined). Working in groups of 30 galaxies per bin produces the average $vz - yz$ colors found in Figure 9 where the error bars are the range of the data, not the error on the mean. The solid line is the CMR for the Coma/Fornax sample, the dotted line is the expected CMR for the changes in luminosity and color as predicted by the SED models. Also shown is an axis of mean Fe/H as would be converted from $vz - yz$ using globular cluster calibrations.

While the range per data point is large, all the binned data points lie below the Coma/Fornax CMR in the expected direction for color evolution. Note that each individual bin does not carry sufficient statistical significance to support a claim of color evolution, but the entire set of all luminosities is statistically significant and a new fit through the averaged data produces a linear relation that is shifted almost exactly in the manner predicted by the models for a passive evolving population. While the large scale cosmological impact of this result is small (the lookback time to A2125 and A2218 are too small to deduce the formation epoch of the red population), the technique does provide some hope of using the CMR at very high redshifts to study, in detail, the star formation history of ellipticals (Ellis *et al.* 1997).

3.7. Blue Fraction

The choice of A2125 and A2218 for deep narrow band imaging was made primarily because these two rich clusters lie at similar intermediate redshifts, yet present contrasting global cluster populations. A2218 is denser than A2125 and has a more compact core population of red galaxies, although the total richness for both clusters is similar. A2125 is more irregular in cluster structure (BM type II-III) than A2218 (BM type II), where cluster shape is considered to be a measure of its dynamical state. In the original work on the Butcher-Oemler effect, A2125 has a higher blue fraction ($f_B=0.17$) compared to A2218 ($f_B=0.11$), although both have blue fractions greater than the value for nearby clusters ($f_B=0.04$) and it is the blue fraction that signals an evolutionary effect in intermediate redshift clusters.

Determining the blue fraction, f_B , is a selection driven process. The original f_B criteria used the

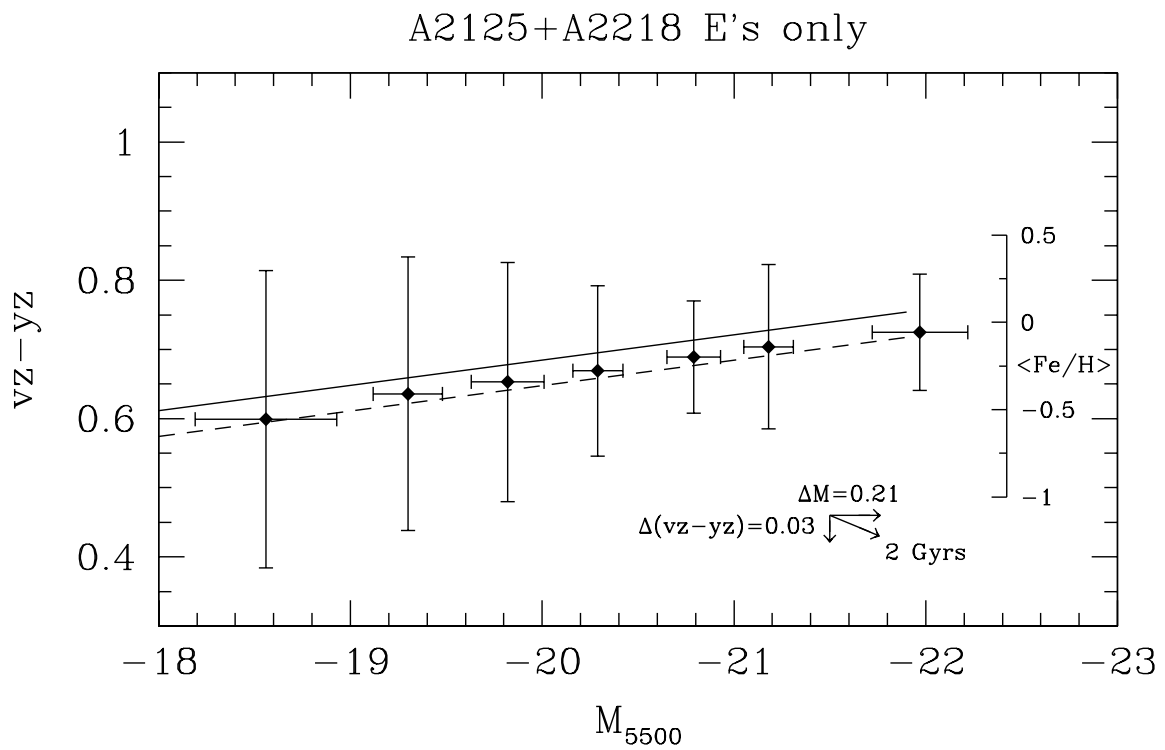


Fig. 9.— The metallicity CMR for class E galaxies in A2125 and A2218. The data has been binned into groups of 30 galaxies with the mean color and luminosity shown as solid symbols. The solid line is the CMR for Coma, the dashed line is the expected change in the CMR due to color evolution for a 2 Gyrs lookback time. Also shown is the metallicity scale from Rakos & Schombert (2004) for the $vz - yz$ color convolved to our multi-metallicity models.

number of galaxies that were a set color difference from the ridgeline of the cluster as a whole. As discussed in Rakos & Schombert (1995), the best color for selecting the blue population in a cluster is $bz - yz$ since the CMR for $bz - yz$ is flat. In any metallicity sensitive color, such as $vz - yz$, a deeper limiting magnitude will introduce relatively bluer (i.e. lower mean metallicity) galaxies. For $bz - yz$, this effect is minimal (although presumably because there is a competing age effect for low mass ellipticals, see §3.5) and, through an analysis of low redshift spirals and irregulars, we have found that the Butcher & Oemler criteria corresponds to a color cutoff of $bz - yz = 0.2$ in our rest frame system (Rakos, Maindl & Schombert 1996). Applying this color criteria, and the using the same limiting magnitude as Butcher & Oemler ($M_{5500} < -20$), results in f_B values of 0.15 and 0.06 for A2125 and A2218 respectively. This is similar to the original Butcher & Oemler values, with A2125 having a richer blue population than A2218.

A simple luminosity cutoff ignores the additional information offered by our four filter photometry system. Our data includes a much deeper sample of galaxies than the original Butcher & Oemler work and our filter system allows us finer discrimination by color. To this end, Figures 10 and 11 display the blue fraction, f_B , as a function of absolute luminosity for A2125 and A2218 (bottom panels). These values are based on the same color cutoff discussed above, only applied to magnitude bins selected to have equal numbers of galaxies per bin. The blue line represents the total f_B for the sample brighter than $M_{5500} = -20$, the original Butcher-Oemler criteria. The full sample displays some interesting trends. For example, both A2125 and A2218 follow the same pattern of an increasing blue fraction with decreasing luminosity (Dahlen, Fransson & Naslund 2001, De Propris *et al.* 2004). In fact, when using the entire sample, A2125 and A2218 have identical f_B values of 0.19 due to the increase in blue galaxies at low luminosities. It is also obvious that the blue fraction for the top three luminosity bins is very low, near 0.05, which is the value for Coma. Therefore, most of the blue population is composed of galaxies fainter than -21.5 .

This result does not imply that cluster populations of A2125 and A2218 are identical to Coma at the bright end of the luminosity function. Even though the blue fraction is low above -21.5 , there are a significant number of bright blue galaxies (see CMR in Figures 6 and 7) that have no counterparts in Coma (see Figure 3 of Odell, Schombert & Rakos 2002). For comparison, the same analysis can be performed using photometric classifications as discussed in §3.1. The top panels in Figures 10 and 11 display the fraction of E, S-, S and S+ type galaxies as a function of absolute luminosity. The trend here is clearer than with the blue fraction such that there is a steady decrease in the fraction of E types with decreasing luminosity matched by an increase in S and S+ types. The transition S- type remains nearly constant. This trend is identical in A2125 and A2218, despite the differences in the density and richness.

Our interpretation of these trends in color and photometric class derives from comparison with nearby clusters (Coma and Fornax) and several intermediate redshift clusters with strong blue populations (A115, A2283, A2317, Rakos *et al.* 2000). In the intermediate redshift clusters, the blue population divides itself into two sub-populations, 1) a bright population with spiral colors and 2) a fainter, dwarf starburst population ($SFR > 10 M_{\odot} \text{ yr}^{-1}$). Consistently, for all the intermediate redshift clusters we have studied, there is a deficiency in blue galaxies in the luminosity range from -20 to -21 compared to the red population, hence a decrease in f_B over these luminosities. Both A2125 and A2218 differ from this trend by lacking a dominate, bright blue population ($M_{5500} < -20$), although they still have a number of starburst galaxies (e.g. C153). In the next section, we will explore the properties of

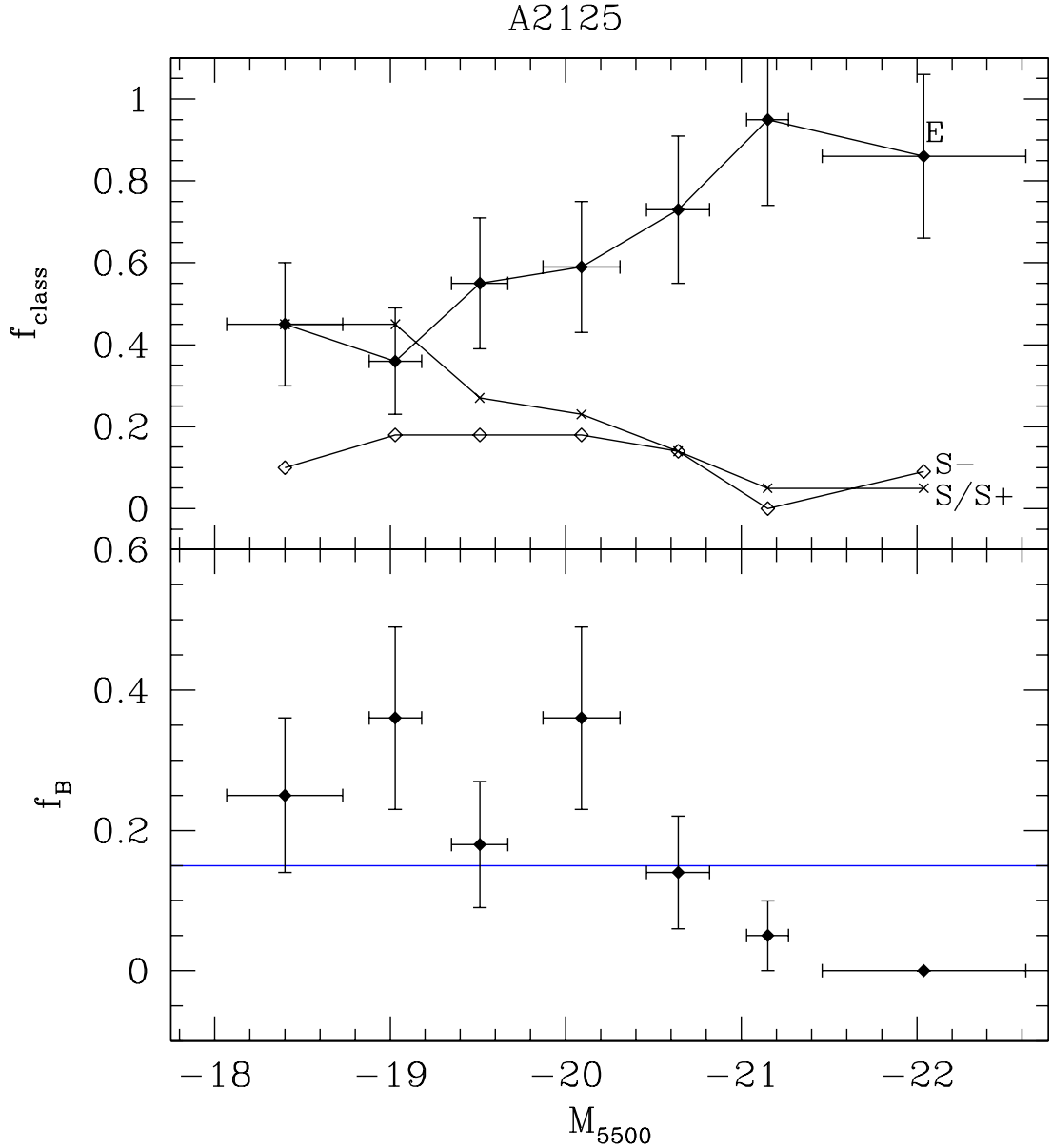


Fig. 10.— The blue fraction (f_B) and photometric class fraction as a function of absolute luminosity for A2125. The blue line represents the cluster f_B as defined by the Butcher-Oemler criteria. As noted in other Butcher-Oemler clusters, the blue population increases its contribution at lower luminosities. The top panel displays the run of photometric classes with absolute magnitude. A decrease in the E class is matched by an increase in S and S+ class objects. The lack of change in the S- population indicates that the switch from star-forming to passive colors is abrupt.

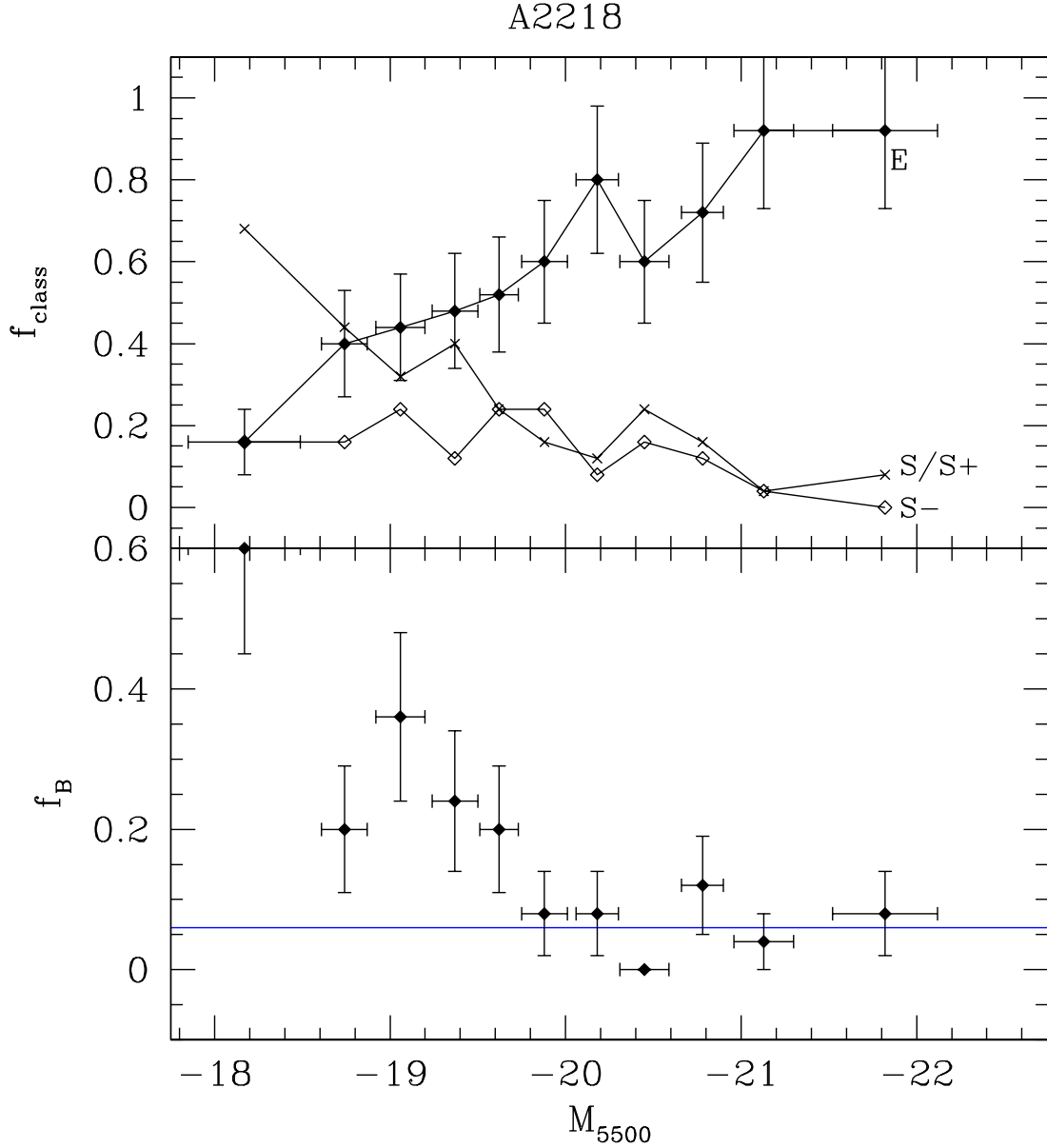


Fig. 11.— The blue fraction (f_B) and photometric class fraction as a function of absolute luminosity for A2218. The blue line represents the cluster f_B as defined by the Butcher-Oemler criteria. The trends are similar to Figure 10, with fewer blue galaxies near the Butcher-Oemler cutoff of $M_{5500} = -20$. This results in a lower global value of f_B for A2218 compared to A2125 even though both clusters have a well developed population of low luminosity blue galaxies.

the blue population in order to understand its origin.

3.8. Properties of the Blue Populations

Given the similarity in trends found in Figures 10 and 11, the question arises of how do the two clusters distinguish themselves with respect to their blue fractions and the state of the Butcher-Oemler effect. Most photometric surveys do not sample deep enough into the luminosity function to allow the faint blue population to significantly contribute to the f_B value, although certainly some of the range and scatter in f_B from cluster to cluster is due to differing magnitude cutoffs and different filter systems. Inspection of the CMR for A2125 and A2218 in Figures 6 and 7 show that the blue galaxies at the high end of the luminosity function are due to galaxies with spiral-like colors in A2218, however, in A2125, we find a majority of the brightest blue galaxies have starburst colors.

This can also be seen in the physical morphology of the blue population from the WFPC2 images. In Table 2, it can be seen that all the blue galaxies in A2125 are late-type Sc and Irr's. However, in A2218, a majority of the blue galaxies (60%) are early-type S0's or Sa/Sb by morphology. Figures 12 and 13 presents a mosaic of a few of the brightest blue galaxies in A2125 and A2218. The blue galaxies in A2218 follow the trends for the Hubble sequence in nearby galaxies, meaning the bluest systems have the latest Hubble classes. For example, #22 and #481 are early-type spirals, #75 and #164 are late-type. The blue galaxies in A2125, in general, are more disturbed from the standard Hubble sequence. Galaxy #481 in A2125 is the well studied starburst C153 (Wange *et al.* 2004) whose optical and HI morphology is distorted as it plows into the cluster ICM. The primary difference between A2125 and A2218 versus Coma is that fact that there are no counterparts in Coma to galaxies shown in Figures 12 and 13. The closest Coma galaxy with colors of a star-forming object has a luminosity of only -18.5 (galaxy A014 in Odell, Schombert & Rakos 2002).

This is the essence of the Butcher-Oemler effect, meaning the difference between clusters with an active Butcher-Oemler population (i.e. A2125) and ones which display a higher fraction of galaxies with spiral-like star formation rates simply due to cosmological time (i.e. A2218). For A2125, there are many indications that the Butcher-Oemler population is linked to the dynamical state of the cluster by the interaction between gas-rich galaxies and the cluster environment either through gas stripping (Gunn & Gott 1972) or the cluster tidal field (Moore *et al.* 1996). Compared to A2218, a more relaxed cluster, the difference in their blue populations lies in the late-type, starburst systems, such as galaxy #481, which have strong evidence of environmentally induced star formation. Removing the starburst systems from A2125 would produce blue fractions similar to A2218. This is not to say that the blue population in A2218 is insignificant for, as with A2125, the blue galaxies in Figure 12 have no counterparts in the core of Coma. However, the blue galaxies in their appearance are consistent with present-day Hubble types and their colors match normal spirals. So even at lookback times of only 2 Gyrs ago, there are significant differences in the cluster populations of rich clusters both in the properties of the S0's (higher fraction of bulge+disk systems) and the blue galaxies (higher fraction of late-type systems).

The high richness of A2125 and A2218 also allows us to test the change in galaxy population with cluster radial distance. Figure 14 displays the distribution of different galaxies types as projected onto the sky. In both clusters it is obvious that the early-type galaxies (E and S-) are strongly clustered in the core and that the late-type galaxies (S and S+) are more evenly distributed. This has been demonstrated

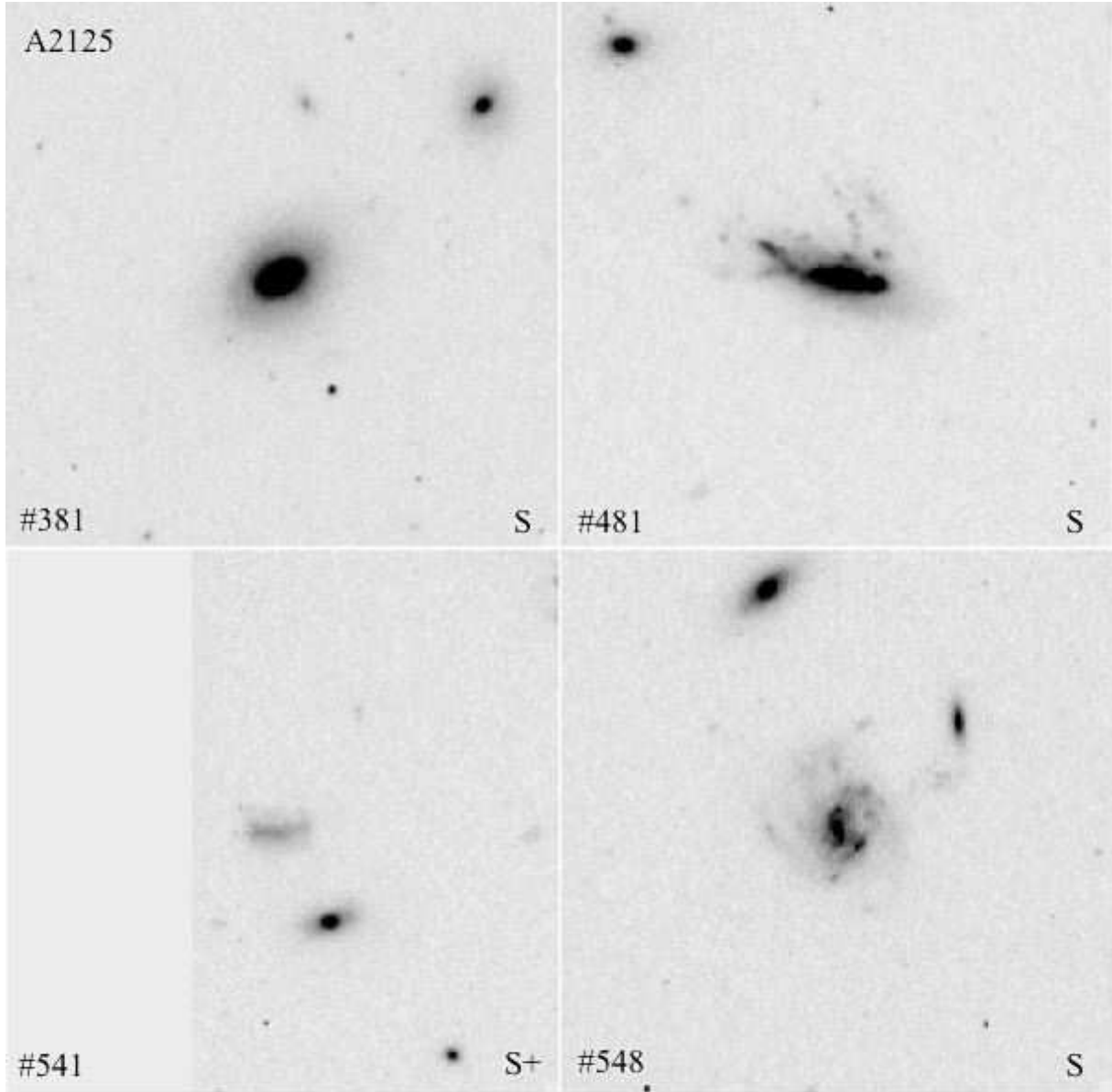


Fig. 12.— A mosaic of four of the brighter blue galaxies in A2125 from WFPC2 imaging (F606W). Each subimage is 50 kpc wide. Galaxy's #381 and #481 are early-type spirals, #541 and #548 are late-type. The blue galaxies in A2125, in general, are more disturbed from the standard Hubble sequence. Galaxy #481 in A2125 is the well studied starburst C153 (Wange *et al.* 2004) whose optical and HI morphology is distorted as it plows into the cluster ICM.

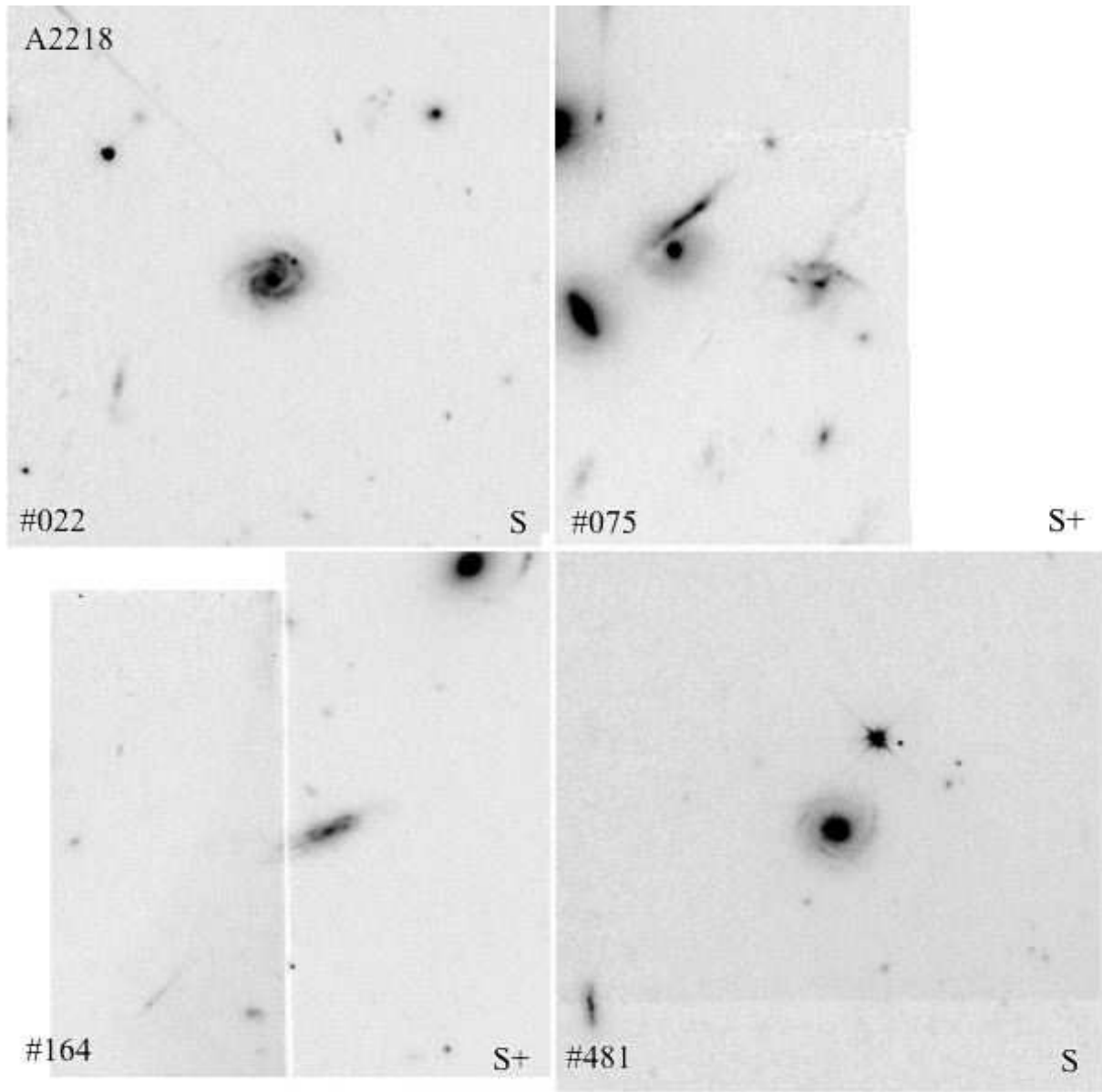


Fig. 13.— A mosaic of four of the brighter blue galaxies in A2218 from WFPC2 imaging (F606W). Each subimage is 50 kpc wide. The blue galaxies in A2218, in general, are follow the standard Hubble sequence, galaxy #075 is an exception to this rule being a highly disturbed, interacting system.

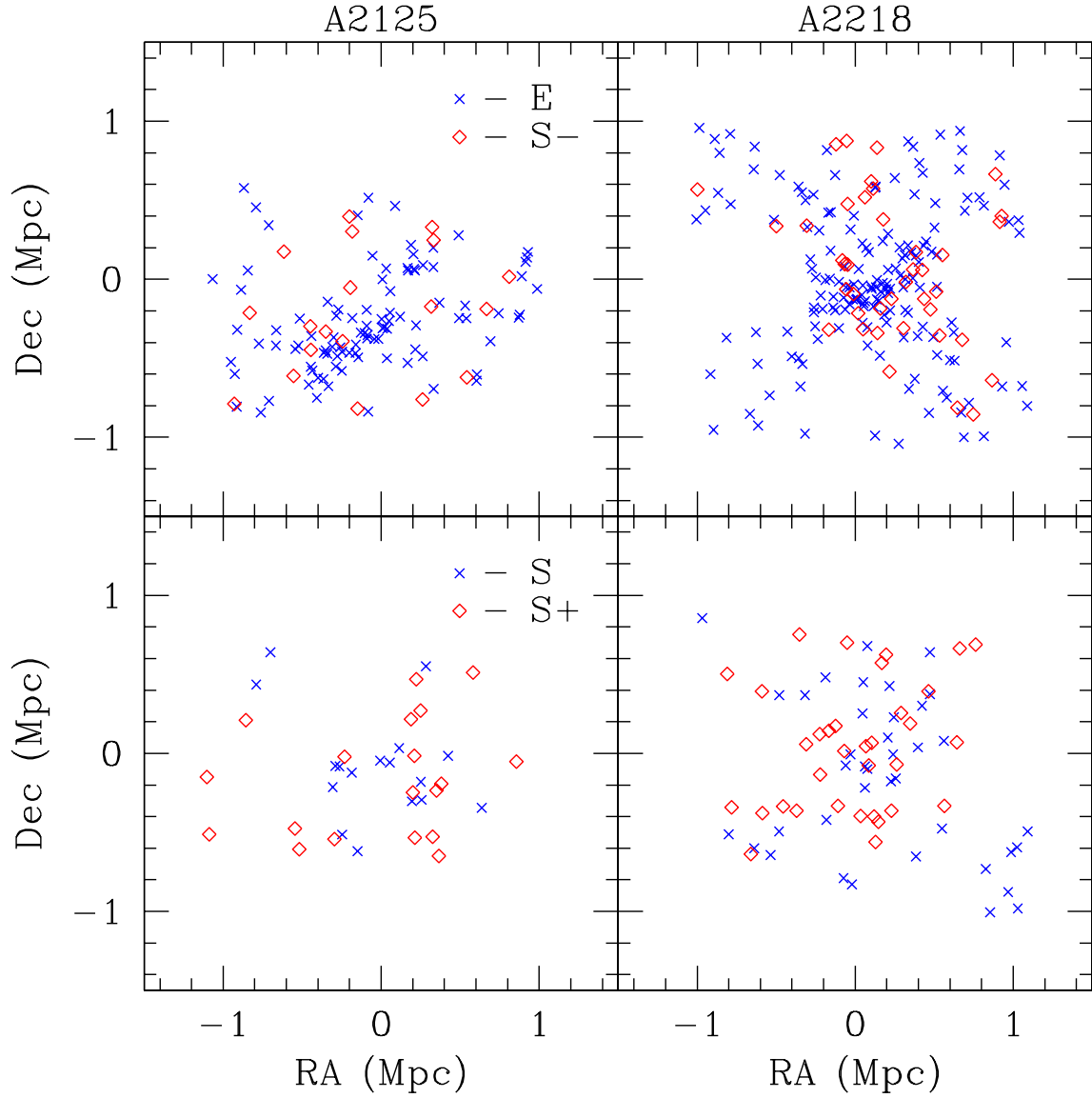


Fig. 14.— The position location of all four photometric classes in A2125 and A2218. Only the E class displays a clear central concentration, the other three classes are evenly distributed throughout the clusters.

in numerous papers (Abraham *et al.* 1996, Ellingson *et al.* 2001) that the blue population is more dense in the outlying regions of a cluster, presumably infalling field galaxies. Thus, one origin hypothesis to the blue population is that they are composed of gas-rich field systems which infall into a dense cluster and environmental influences produce a starburst. However, notable counterexamples, such as galaxy #481 (aka C153 in A2125), indicate that some of the starburst systems near the cluster core are undergoing of a strong interaction with the dense ICM and are not simply an infalling field population.

The radial distance effect on the blue population can be seen in more detail in Figures 15 and 16, the $uz - yz$ CMR divided into three bins of radial distance from the center center. Both A2125 and A2218 display a lack of any bright blue galaxies in their cluster cores, with an increase in the number of blue galaxies, and their mean luminosity, at larger radii. We note that these trends are identical in both clusters despite their differences in cluster structure and dynamical state. In fact, aside from a slightly higher fraction of starburst systems in A2125, neither cluster can be distinguished from each other based on the distribution of their blue populations.

4. CONCLUSIONS

One of the main obstacles in the study of galaxy evolution is the wide range of environmental effects on the star formation and morphological history of galaxies. Given the diversity of environments in which galaxies are found, and the importance that environment plays in our galaxy formation scenarios, predicting the evolution of particular systems may elude our understanding for the near future. In this study, we have attempted to minimize the range of evolutionary effects by comparing two rich clusters at similar redshifts, yet relatively short lookback times, to dense present-day clusters (i.e. Coma). While investigating galaxy populations at redshifts of 0.2 will not reveal a great deal of information concerning formation epoch, it does allow us to test passive evolution models and determine the characteristics of this epoch's dying blue population.

We divide our results into three parts: 1) the raw observables, 2) model dependent interpretation of those observables and 3) speculation on the meaning of the data. The first two, our primary observables and interpretation of the data, are summarized in the following list:

- Our four color filter system allows the spectrophotometric classification of the galaxy sample using principal component analysis. We have broken the sample into four color groups, E, S-, S and S+ in order of increasing blueness due to star formation. A non-thermal color contribution can also be detected in the PC2 axis (class A), although, not surprisingly, these objects are very rare in our sample. The classification results are summarized in Table 1, A2125 and A2218 are very similar in their photometric properties, both being richer in blue galaxies compared to Coma. Even the core regions of A2125 and A2218 have a higher fraction of blue galaxies compare to the core of Coma, despite the higher galaxy densities for A2125 and A2218.
- Archive WFPC2 imaging allows the morphological classification of a subset of the photometric sample (32% of the total sample). Typically, these galaxies are in the cluster cores due to observing constraints. The relationship between visual morphology and photometric classification is shown in Table 2. As expected, there is a tight correlation between photometric classification by color and morphology. Only a few early-type disk galaxies are classified as red (E or S-) and all the

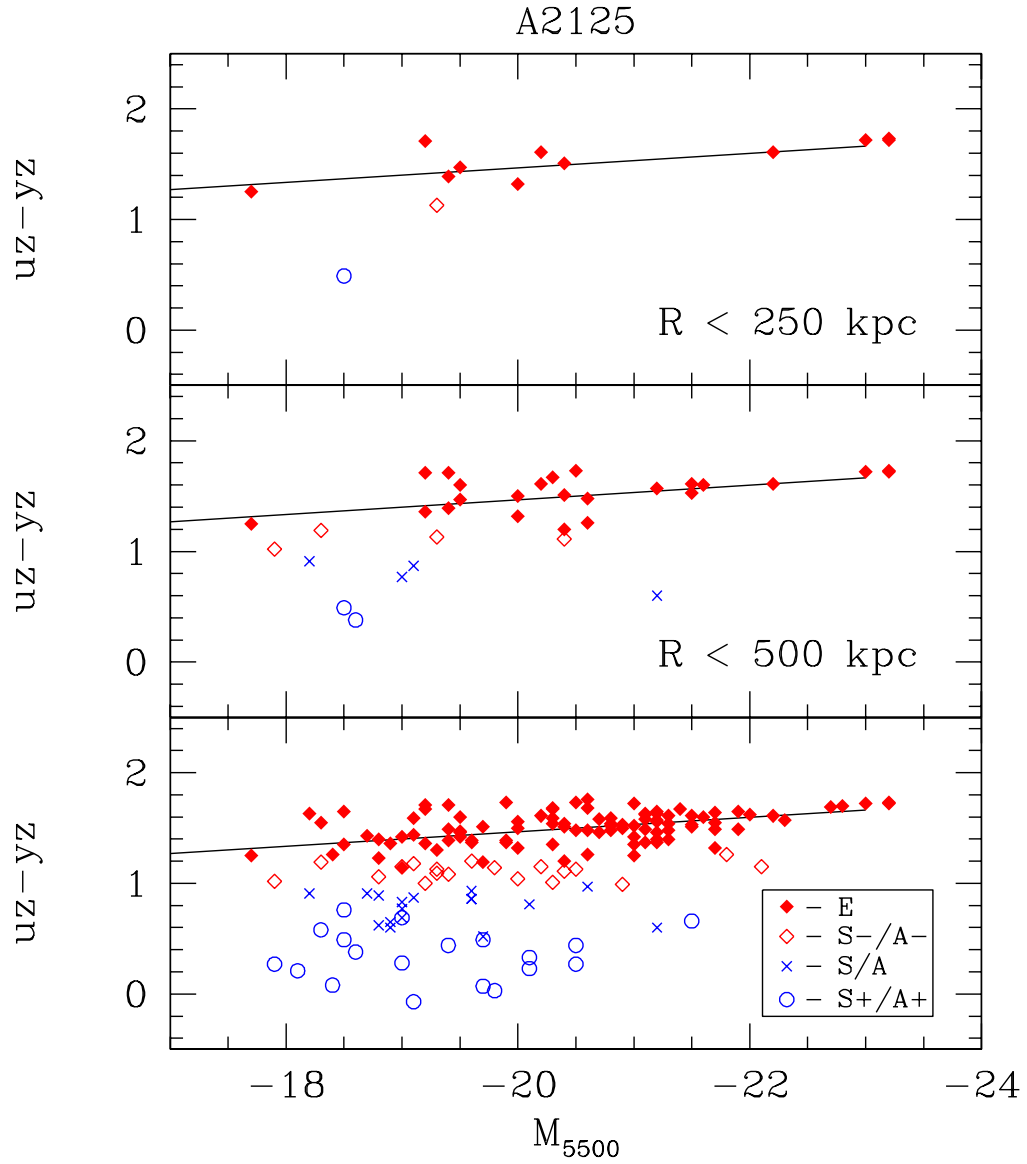


Fig. 15.— The $uz - yz$ CMR as a function of cluster distance in A2125. The increase in the number of blue galaxies with radius is evident. There is no change in the red population with radius with respect to the CMR slope, although an increase number of transition objects (S-) would complicate the fit by morphology alone.

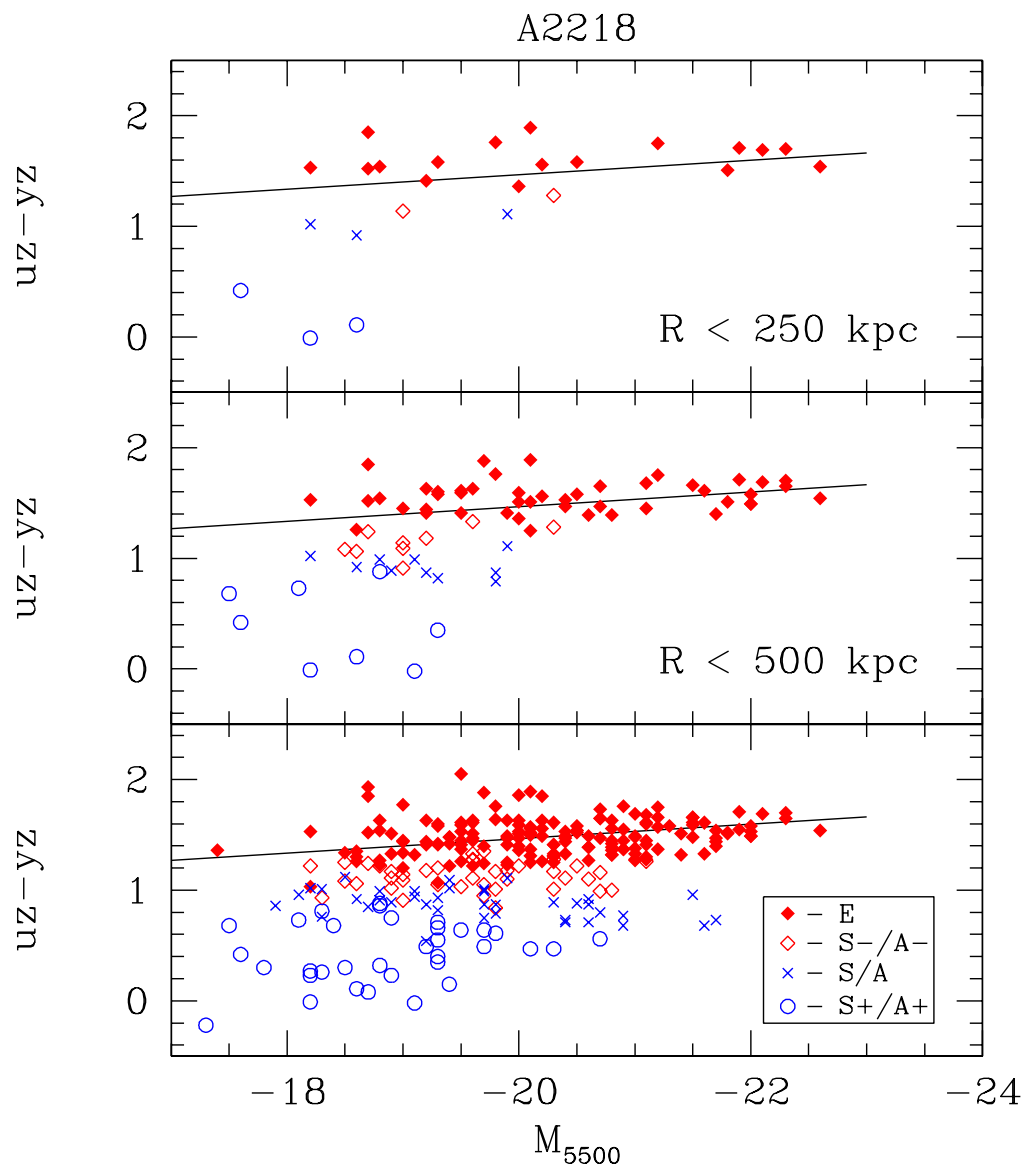


Fig. 16.— The $uz - yz$ CMR as a function of cluster distance in A2218.

blue systems display late-type morphology. It is not the case that the blue galaxies are fading into large bulge S0's, as most are late-type systems (see also Couch *et al.* 1998). There is a noticeable deficiency in ellipticals ($r^{1/4}$ shaped objects) of about 15% compared to Coma, which matches in increased number of late-type galaxies. However, the differences in the S0 population (see below) indicate that the conversion of S0's to ellipticals is matched by the conversion of late-type galaxies to S0's.

- Detailed surface photometry could be performed on the WFPC2 images down to 28 mag arcsecs $^{-2}$ and the resulting surface brightness profiles are divided into three types; 1) $r^{1/4}$ shape profiles (B), 2) combination of $r^{1/4}$ shape bulge and exponential disk (B+D) and 3) pure exponential disk (D). Table 3 and 4 summarizes the relationship between surface brightness profile classification and photometric classification and morphology. As expected, the blue population is almost completely composed of disk galaxies with a few bulge+disk objects. The red population is composed of a mixture of B, B+D and D systems in a average ratio of 25%:40%:10% of the total cluster population. This differs significantly from Coma's 40%:20%:30% mixture. An increase of red pure disk galaxies (lenticulars) may arise from faded blue galaxies; however, the increase in B systems and the decrease in B+D systems can only arise if 1/2 of the S0's at intermediate redshift are converted, structurally, into ellipticals. This can also be seen in Table 4 where approximately 80% of the S0's in A2125 and A2218 are bulge+disk systems, whereas only 35% of the S0's in Coma have this type of structure. The majority of S0's in nearby clusters are lenticulars (van den Bergh 1994), which are a minority at intermediate redshifts.
- The color distributions for the cluster galaxies occupies the same phase space as SDSS galaxies (Smolcic *et al.* 2004) with barely detectable evolutionary effects. The red population follows a strict metallicity-color relation (as compared to SED models). The blue population has colors consistent with nearby galaxies undergoing star formation at rates varying from 1 to $10 M_{\odot}$ per yr. None of the blue galaxies are composed of a pure young stellar population, but rather follow the ‘frosting’ models, a small, young population on top of an older stellar population (i.e. recent star formation).
- The color-magnitude relation for red galaxies follows the same slope and zeropoint as Coma with minor, but detectable, deviations that correspond to direct evidence for color evolution. This consistence to the CMR, plus low scatter is also seen in clusters up redshifts of 0.5 (Ellis *et al.* 1997), places fairly strong constraints on the epoch of star formation for the red population to be greater than a redshift of 5 (the red envelope, see Rakos & Schombert 1995). The lack of a meaningful slope to the $bz - yz$ color argues for an age effect in the direction of older mean age, or later epoch of formation, for lower luminosity ellipticals (see Rakos & Schombert 2004).
- The calculated blue fraction (f_B) varies widely depending on the luminosity and radius cutoffs. Using the original Butcher-Oemler criteria derives a blue fraction of 0.15 for A2125 and 0.06 for A2218, both are higher than typical values for present-day rich clusters. The blue fraction increases with decreasing luminosity and with increasing radius. Both clusters have similar f_B values for the high end of the luminosity function; however, the type of blue galaxies differs between the clusters. In A2218, the colors of these bright blue galaxies indicate normal, spiral-like star formation rates and their morphology from WFPC2 images is consistent with early-type disks. The opposite is true in A2125, most of the brightest blue galaxies display starburst colors and later morphological

types. Thus, the Butcher-Oemler effect is one of both color and morphological evolution.

- An increasing number of starburst colors are found at lower luminosities in both clusters indicating that the Butcher-Oemler population is divided into two sub-populations, a bright, fading spiral population and a faint, starburst dwarf population. We note that interpretations of star formation rate are based on continuum colors (i.e. averaged over the past couple of Gyrs), spectroscopic information at this redshift indicates that spirals are ‘quenched’ in that their emission lines such that current SFR values are lower than normal spirals (Couch *et al.* 1998, Dressler *et al.* 1999, Poggianti *et al.* 1999). It is this comparison between spectral values and continuum colors that makes photometry of distant clusters a necessary component to understanding the evolution of the blue population.

In many ways, the galaxies in A2125 and A2218 are similar to those found in present-day rich clusters. The cores of both clusters are dominated by red, elliptical galaxies despite the clear dynamical differences between the irregular A2125 and the cD dominated A2218. The red populations (ellipticals and S0’s) follow the same mass-metallicity relationship as Coma and Fornax and even display the correct amount of evolution in color and luminosity expected from passive evolution models. It is interesting to note that both Coma and Fornax, in the present epoch, and A2125 and A2218, two Gyrs in the past, have a flat $bz - yz$ CMR. The SED models predict a small but detectable slope from the metallicities implied by the $uz - yz$ and $vz - yz$ colors. The lack of a slope in Figures 6 and 7 imply an age effect that is coupled to the metallicity of a galaxy (the direction is such that metal-poor, or low mass, galaxies are older). If an age effect is responsible for the $bz - yz$ CMR, then the estimated age difference from low to high mass is small, less than 2 to 3 Gyrs (see Rakos & Schombert 2004).

A change in mean age of a stellar population with mass has three possible interpretations: 1) lower mass galaxies form before high mass galaxies, 2) all galaxies form at the same time, but high mass galaxies have an extended period of star formation that produces a younger mean age or 3) higher mass galaxies acquire a younger stellar population through mergers or cannibalism. Hierarchical models of galaxy formation favor the first scenario; however, the mass-metallicity relation, seen so clearly in the $uz - yz$ and $vz - yz$ CMR, makes a process of building high metallicity, high mass galaxies from low metallicity, low mass galaxies problematic. Certainly more gas mass in high mass galaxies implies a longer star formation epoch, but the CMR is best explained by an abrupt halt to star formation by galactic winds and, thus, extending the time of star formation beyond a single Gyr is also difficult to match to the CMR. Lastly, galaxy cannibalism is present in clusters (Schombert 1987), but the number of star-forming galaxies in a cluster core to accrete is limited and previous work (Kuntschner 2000, Trager *et al.* 2000) has demonstrated that cluster ellipticals are as old as globular clusters with very few examples of ellipticals with a younger population mixed into the original stellar population.

In agreement with the conclusions on distant clusters by Dressler *et al.* (1997), the red population in A2125 and A2218 appears to predate the formation of the cluster environment and its color properties appear to be independent of the cluster dynamical state. The key difference between the cluster populations in A2125 and A2218 lies in the properties of the blue population. Although this was only a sample of two clusters, the more dynamically relaxed (A2218) cluster’s blue population has fewer starburst systems than the less dynamically evolved (A2125) cluster. And many of those starburst galaxies show clear signs of environmentally induced star formation (see Wange *et al.* 2004) such that the age of the stellar population in blue cluster galaxies is linked to the dynamical state of the cluster.

When we compare all the galaxy properties (color and structure) we also find differences in the S0 population. A majority of the S0's in A2125 and A2218 are B+D type galaxies by structure, meaning they have detectable bulge and disk combinations. However, these types of S0's are rare in Coma where a majority of the S0 population is comprised of pure disk systems (i.e. lenticulars). A clue to where the B+D S0's have gone lies in Figure 2, a plot of the structure parameters of the $r^{1/4}$ parts of the red population (ellipticals and bulges). The structure of elliptical galaxies in A2125 and A2218 follow the same effective radius (r_e) versus effective surface brightness (μ_e) relations as nearby cluster ellipticals. The bulges of B+D S0's also follow the elliptical relation (i.e. they are structurally identical to ellipticals). This suggests that many of the S0's at intermediate redshift are stripped of their disks (either by encounters with other galaxies or by the cluster tidal field) and their remaining bulges become ellipticals.

Lastly, we comment on the apparent special time that we live in with respect to galaxy evolution. One of the philosophical difficulties with the Butcher-Oemler effect is that we appear to live at just the right epoch were star formation has (recently) ended in cluster cores. This would appear, at first, to be a violation of the Copernican principle, applied in a temporal fashion. However, the Universe does evolve. Certainly, we expect to find observers only at a cosmic epoch that can support complex lifeforms (Davies 2004). Once a galaxy's gas supply is exhausted, it will rapidly take on a smooth appearance and red colors (i.e. S0-like). Thus, the Butcher-Oemler effect is merely a statement of the gas supply in various clusters and the rapid nature that various cluster environmental effects can have on a particular galaxy. It is also a mistake to assume that the Butcher-Oemler effect is one of decreasing blue fraction to present-day values. There are numerous present-day clusters with large blue galaxy populations (e.g. Hercules A2151) and the evolutionary process is not finished in those clusters. There is insufficient information on the projected course of cluster populations to conclude that today represents a final state in cluster evolution.

Financial support from Austrian Fonds zur Foerderung der Wissenschaftlichen Forschung and NSF grant AST-0307508 is gratefully acknowledged. Some of the data presented in this paper were obtained from the Multimission Archive at the Space Telescope Science Institute (MAST). STScI is operated by the Association of Universities for Research in Astronomy, Inc., under NASA contract NAS5-26555. Support for MAST for non-HST data is provided by the NASA Office of Space Science via grant NAG5-7584 and by other grants and contracts. This research has made use of the NASA/IPAC Extragalactic Database (NED) which is operated by the Jet Propulsion Laboratory, California Institute of Technology, under contract with the National Aeronautics and Space Administration. We thank KPNO for the usual dribble of telescope time for this project and the mountain staff for their efforts during the observing runs. We also thank the anonymous referee for his/her time in proofing this paper.

REFERENCES

Abraham, R., va, den, Glazebrook, K., Ellis, R., Santiago, B., Surma, P. & Griffiths, R. 1996, ApJS, 107, 1

Abraham, R. 1999, Ap&SS, 269, 323

Andreon, S. 1998, ApJ, 501, 533

Andreon, S. 2003, A&A, 409, 37

Andreon, S. 1998, ApJ, 501, 533

Aragon-Salamanca, A., Ellis, R., Couch, W. & Carter, D. 1993, MNRAS, 262, 764

Arimoto, N. & Yoshii, Y. 1987, A&A, 173, 23

Bender, R., Burstein, D. & Faber, S. 1992, ApJ, 399, 462

Bower, R., Lucey, J. & Ellis, R. 1992, MNRAS, 254, 589

Bruzual, G. & Charlot, S. 2003, MNRAS, 344, 1000

Butcher, H. & Oemler, A., 1978, ApJ, 226, 559

Couch, W., Barger, A., Smail, I., Ellis, R. & Sharples, R. 1998, ApJ, 497, 188

Couch, W., Balogh, M., Bower, R., Smail, I., Glazebrook, K. & Taylor, M. 2001, ApJ, 549, 820

Dahlen, T., Fransson, C. & Naslund, M. 2002, MNRAS, 330, 167

Davies, P. 2004, astro-ph/0403047

De Propris, R. and 29 co-authors 2004, MNRAS, 351, 125

Dressler, A. 1980, ApJS, 42, 565

Dressler, A. & Gunn, J. 1982, ApJ, 263, 533

Dressler, A., Oemler, A., Couch, W., Smail, I., Ellis, R., Barger, A., Butcher, H., Poggianti, B. & Sharples, R. 1997, ApJ, 490, 577

Dressler, A., Smail, I., Poggianti, B., Butcher, H., Couch, W., Ellis, R. & Oemler, A., 1999, ApJS, 122, 51

Dressler, A. 2003, *Star Formation Through Time*, ASP Conference Proceedings, Vol. 297, p. 203

Eggen, O., Lynden-Bell, D. & Sandage, A. 1962, ApJ, 136, 748

Ellingson, E., Lin, H., Yee, H. & Carlberg, R. 2001, ApJ, 547, 609

Ellis, R., Smail, I., Dressler, A., Couch, W., Oemler, A., Butcher, H. & Sharples, R. 1997, ApJ, 483, 582

Faber, S. 1973, ApJ, 179, 731

Fasano, G., Poggianti, B., Couch, W., Bettoni, D., Kjærgaard, P. & Moles, M. 2000, ApJ, 542, 673

Goto, T., Okamura, S., Yagi, M., Sheth, R., Bahcall, N., Zabel, S., Crouch, M., Sekiguchi, M., Annis, J. & Bernardi, M. 2003, PASJ, 55, 739

Gunn, J. & Gott, J. 1972, ApJ, 176, 1

Larson, R. 1974, MNRAS, 166, 585

Jones, L., Smail, I. & Couch, W. 2000, ApJ, 528, 118

Kauffmann, G. 1996, MNRAS, 281, 487

Kauffmann, G. & Charlot, S. 1998, MNRAS, 294, 705

Kneib, J., Ellis, R., Smail, I., Couch, W. & Sharples, R. 1996, ApJ, 471, 643

Kodama, T., Arimoto, N., Barger, A. & Aragón-Salamanca, A. 1998, A&A, 334, 99

Kormendy, J. 1980, *Proc. ESO Workshop on Two-Dimensional Photometry*, p. 191

Kuntschner, H. 2000, MNRAS, 315, 184

MacArthur, L., Courteau, S., Bell, E. & Holtzman, J. 2004, ApJS, 152, 175

Margininer, V., d, Carvalho, Gal, R. & Djorgovski, S. 2001, ApJ, 548, L143

Moore, B., Katz, N., Dressler, A. & Oemler, A. 1996, MNRAS, 379, 613

Odell, A., Schombert, J. & Rakos, K. 2002, AJ, 124, 3061

Pahre, M. 1999, ApJS, 124, 127

Pimbblet, K. 2003, PASA, 20, 294

Poggianti, B., Bridges, T., Carter, D., Mobasher, B., Doi, M., Kashikawa, N., Komiyama, Y., Okamura, S. & Sekiguchi, M. 2001, ApJ, 563, 118

Poggianti, B., Smail, I., Dressler, A., Couch, W., Barger, A., Butcher, H., Ellis, R. & Oemler, A., 1999, ApJ, 518, 576

Rakos, K., Maindl, T. & Schombert, J. 1996, ApJ, 466, 122

Rakos, K. & Schombert, J. 1995, ApJ, 439, 47

Rakos, K., Schombert, J., Odell, A. & Steindling, S. 2000, ApJ, 540, 715

Rakos, K., Schombert, J., Maitzen, H., Prugovecki, S. & Odell, A. 2001, AJ, 121, 1974

Rakos, K. & Schombert, J. 2004, AJ, 127, 1502

Rakos, K. & Schombert, J., 2005, PASP, in press

Schombert, J. 1986, ApJS, 60, 603

Schombert, J. 1987, ApJS, 64, 643

Schombert, J. 2005, in prep.

Schulz, J., Fritze-v, Alvensleben, Moumller, C. & Fricke, K. 2002, A&A, 398, 89

Smail, I., Kuntschner, H., Kodama, T., Smith, G., Packham, C., Fruchter, A. & Hook, R. 2001, MNRAS, 323, 839

Smolcic, V., Ivezic, Z., Gacesa, M., Rakos, K., Pavlovski, K., Ilijic, S., Lupton, R., Schlegel, D., Kauffmann, G., Tremonti, C., Brinchmann, J., Charlot, S., Heckman, T., Knapp, G. & Gunn, J. 2004, MNRAS, in press

Stanford, S., Eisenhardt, P. & Dickinson, M. 1998, ApJ, 492, 461

Steindling, S., Brosch, N. & Rakos, K. 2001, ApJS, 132, 19

Trager, S., Faber, S., Worthey, G. & Gonzalez, J. 2000, AJ, 120, 165

van den Bergh, S. 1990, ApJ, 348, 57

van den Bergh, S. 1994, AJ, 107, 153

van Dokkum, P., Stanford, S., Holden, B., Eisenhardt, P., Dickinson, M. & Elston, R. 2001, *Astrophys. Lett.*, 552, 101

Visvanathan, N. & Sandage, A. 1977, ApJ, 216, 214

Wang, D., Owen, F., Ledlow, M. & Keel, W. 2004, astro-ph/0404313

Ziegler, B., Bower, R., Smail, I., Davies, R. & Lee, D. 2001, MNRAS, 325, 1571

Table 1. Population Fractions by Photometric Classification

Type	A2125	A2125 (core) ^a	A2218	A2218 (core) ^a	Coma (core) ^a
E	0.64	0.73	0.60	0.72	0.93
S-/A-	0.12	0.11	0.14	0.10	0.02
S/A	0.11	0.11	0.14	0.10	0.04
S+/A+	0.13	0.05	0.12	0.08	0.02

Note. — ^a $R < 500$ kpc

Table 2. WFPC2 Population Fractions by Morphology and Photometric Classification

Type	E (%)	S0 (%)	Sa/Sb (%)	Sc/Irr (%)	Totals (%)
<u>A2125</u>					
E	23.1	57.7	7.7	0.0	88.5
S-/A-	0.0	0.0	0.0	0.0	0.0
S/A	0.0	0.0	0.0	7.7	7.7
S+/A+	0.0	0.0	0.0	3.8	3.8
	23.1	57.7	7.7	11.5	
E/S-/A-	23.1	57.7	7.7	0.0	88.5
S/S+	0.0	0.0	0.0	11.5	11.5
A/A+	0.0	0.0	0.0	0.0	0.0
<u>A2218</u>					
E	25.2	37.4	0.0	0.0	62.6
S-/A-	1.9	13.1	0.9	0.0	15.9
S/A	0.0	6.5	5.7	0.9	13.1
S+/A+	0.9	0.0	0.0	7.5	8.4
	28.0	57.0	6.6	8.4	
E/S-/A-	27.1	50.5	0.9	0.0	78.5
S/S+	0.0	2.8	4.7	4.7	12.2
A/A+	0.9	3.7	1.0	3.7	9.3
<u>Coma</u>					
E	40.0	48.3	1.7	0.0	90.0
S-/A-	0.0	1.7	0.0	0.0	1.7
S/A	3.3	1.7	1.7	0.0	6.7
S+/A+	0.0	1.6	0.0	0.0	1.6
	43.3	53.3	3.4	0.0	
E/S-/A-	40.0	50.0	1.7	0.0	91.7
S/S+	1.6	0.0	1.7	0.0	3.3
A/A+	1.7	3.3	0.0	0.0	5.0

Table 3. WFPC2 Population Fractions by Surface Brightness Profile and Photometric Classifications

Type	B (%)	B+D (%)	D (%)	Totals (%)
<u>A2125</u>				
E	23.1	53.8	11.6	88.5
S-/A-	0.0	0.0	0.0	0.0
S/A	0.0	0.0	7.7	7.7
S+/A+	0.0	0.0	3.8	3.8
	23.1	53.8	23.1	
E/S-/A-	23.1	53.8	11.5	88.5
S/S+	0.0	0.0	11.5	11.5
A/A+	0.0	0.0	0.0	0.0
<u>A2218</u>				
E	25.2	34.6	2.8	62.6
S-/A-	1.9	9.3	4.7	15.9
S/A	0.0	7.5	5.6	13.1
S+/A+	0.9	0.9	6.5	8.4
	28.0	52.3	19.6	
E/S-/A-	27.1	43.9	7.5	78.5
S/S+	0.0	3.7	8.4	12.1
A/A+	0.9	4.7	3.7	9.3
<u>Coma</u>				
E	40.0	18.3	31.7	90.0
S-/A-	0.0	0.0	1.7	1.7
S/A	3.3	1.7	1.7	6.7
S+/A+	0.0	0.0	1.7	1.7
	43.3	20.0	36.7	
E/S-/A-	40.0	18.3	33.3	91.7
S/S+	1.7	0.0	1.7	3.3
A/A+	1.7	1.7	1.7	5.0

Table 4. WFPC2 Population Fractions by Surface Brightness Profile and Morphology

Type	B (%)	B+D (%)	D (%)	Totals (%)
<u>A2125</u>				
E	23.1	0.0	0.0	23.1
S0	0.0	50.0	7.7	57.7
Sa	0.0	3.8	3.9	7.7
Sc	0.0	0.0	11.5	11.5
	23.1	53.8	23.1	
<u>A2218</u>				
E	28.0	0.0	0.0	28.0
S0	0.0	46.7	10.3	57.0
Sa	0.0	4.7	1.8	6.5
Sc	0.0	0.9	7.5	8.4
	28.0	52.3	19.6	
<u>Coma</u>				
E	43.3	0.0	0.0	43.3
S0	0.0	18.3	35.0	53.3
Sa	0.0	1.7	1.7	3.4
Sc	0.0	0.0	0.0	0.0
	43.3	20.0	36.7	